



Regulation of host and virus genes by neuronal miR-138 favours herpes simplex virus 1 latency

Boqiang Sun^{1,2,3,11}, Xuewei Yang^{1,2,4,11}, Fujun Hou^{1,2,11}, Xiaofeng Yu^{1,2,5}, Qiongyan Wang^{1,2}, Hyung Suk Oh^{1,6}, Priya Raja⁶, Jean M. Pesola⁷, Emilia A. H. Vanni^{1,7}, Seamus McCarron⁷, Jenna Morris-Love^{1,7,8}, Alex H. M. Ng^{1,9,10}, George M. Church^{1,9,10}, David M. Knipe^{1,6}, Donald M. Coen⁷ and Dongli Pan^{1,2,12}

MicroRNA miR-138, which is highly expressed in neurons, represses herpes simplex virus 1 (HSV-1) lytic cycle genes by targeting viral *ICP0* messenger RNA, thereby promoting viral latency in mice. We found that overexpressed miR-138 also represses lytic processes independently of *ICP0* in murine and human neuronal cells; therefore, we investigated whether miR-138 has targets besides *ICP0*. Using genome-wide RNA sequencing/photoactivatable ribonucleoside-enhanced crosslinking and immunoprecipitation followed by short interfering RNA knockdown of candidate targets, we identified the host *Oct-1* and *Foxc1* messenger mRNAs as miR-138's targets, whose gene products are transcription factors important for HSV-1 replication in neuronal cells. *OCT-1* has a known role in the initiation of HSV transcription. Overexpression of *FOXC1*, which was not known to affect HSV-1, promoted HSV-1 replication in murine neurons and ganglia. CRISPR-Cas9 knockout of *FOXC1* reduced viral replication, lytic gene expression and miR-138 repression in murine neuronal cells. *FOXC1* also collaborated with *ICP0* to decrease heterochromatin on viral genes and compensated for the defect of an *ICP0*-null virus. In summary, miR-138 targets *ICP0*, *Oct-1* and *Foxc1* to repress HSV-1 lytic cycle genes and promote epigenetic gene silencing, which together enable favourable conditions for latent infection.

MicroRNAs (miRNAs) are post-transcriptional regulators of gene expression in eukaryotic cells. In post-embryonic metazoan cells, miRNAs act mainly by reducing target messenger RNA levels via Argonaute (AGO) proteins, thereby extending and reinforcing gene regulatory patterns specified by transcriptional regulation^{1,2}. Virus- and host-encoded miRNAs can also regulate virus infection by targeting individual viral mRNAs, regulating individual host factors or modulating the host's immune response network^{3–6}.

One interesting example of miRNA regulation of virus infection is regulation of herpes simplex virus 1 (HSV-1) latency, where repression of lytic (productive) infection benefits the virus. After lytic infection in peripheral tissues, HSV-1 establishes lifelong latent infection in sensory neurons, thereby evading immune clearance. HSV-1 can reactivate from latency, permitting the spread to new hosts⁷. During lytic infection, viral gene expression proceeds in an ordered cascade. After the viral genome enters the nucleus, the virion-delivered VP16 protein complexes with the cellular proteins HCF-1 and OCT-1 (refs. ^{8,9}). This complex assembles on sequences in immediate-early promoters to recruit factors that drive immediate-early gene transcription. Most immediate-early gene products promote the expression of subsequent classes of viral genes—early and late—with the immediate-early protein ICP0 also providing a positive feedback loop to induce enhanced expression of all classes of genes through its ubiquitin ligase activity^{7,10}. These gene activation events coincide with the removal of histones

associated with incoming viral genomes, the loss of heterochromatin modifications and the gain of euchromatin modifications^{11–14}. During the establishment of latency, lytic promoters become increasingly associated with histones enriched for heterochromatin modifications^{15–19}. When latency is fully established, lytic genes are largely silenced, with the only abundant viral gene products being the latency-associated transcripts⁷ and some viral miRNAs^{20,21}. On reactivation, an early stage of derepression independent of viral proteins is followed by a later stage that produces infectious viral particles through the actions of viral proteins including VP16 (refs. ^{22–25}).

Besides transcriptional regulation, a neuron-specific host miRNA, miR-138, represses ICP0 expression by binding to two sites in the *ICP0* 3' untranslated region (UTR)²⁶. Mutations in these sites increase lytic gene expression in mouse neuronal cells and ganglia and increase mouse mortality, indicating that miR-138 promotes latency by repressing *ICP0*. However, the effects of this miRNA:mRNA interaction are limited, which has contributed to a debate on whether host miRNAs contribute to repression of viral replication^{3–6,27}. To address this issue, we investigated whether miR-138 had additional targets that regulate HSV-1 infection.

Results

miR-138 represses HSV-1 replication independent of ICP0. To investigate the effects of miR-138 on HSV-1 replication, we transfected Neuro-2a cells (mouse brain neuroblastoma cells) with miRNA mimics before infection with 1 of 3 viruses: wild-type (WT)

¹Department of Medical Microbiology and Parasitology, Zhejiang University School of Medicine, Hangzhou, China. ²Department of Infectious Diseases of Sir Run Run Shaw Hospital, Zhejiang University School of Medicine, Hangzhou, China. ³Thermo Fisher Scientific, Shanghai, China. ⁴Innovent Biologics, Inc., Suzhou, China. ⁵Zhejiang Chinese Medical University, Hangzhou, China. ⁶Department of Microbiology, Blavatnik Institute, Harvard Medical School, Boston, MA, USA. ⁷Department of Biological Chemistry and Molecular Pharmacology, Blavatnik Institute, Harvard Medical School, Boston, MA, USA. ⁸Graduate Program in Pathobiology, Brown University, Providence, RI, USA. ⁹Wyss Institute for Biologically Inspired Engineering, Harvard University, Cambridge, MA, USA. ¹⁰Department of Genetics, Blavatnik Institute, Harvard Medical School, Boston, MA, USA. ¹¹These authors contributed equally: Boqiang Sun, Xuewei Yang, Fujun Hou. e-mail: pandongli@zju.edu.cn

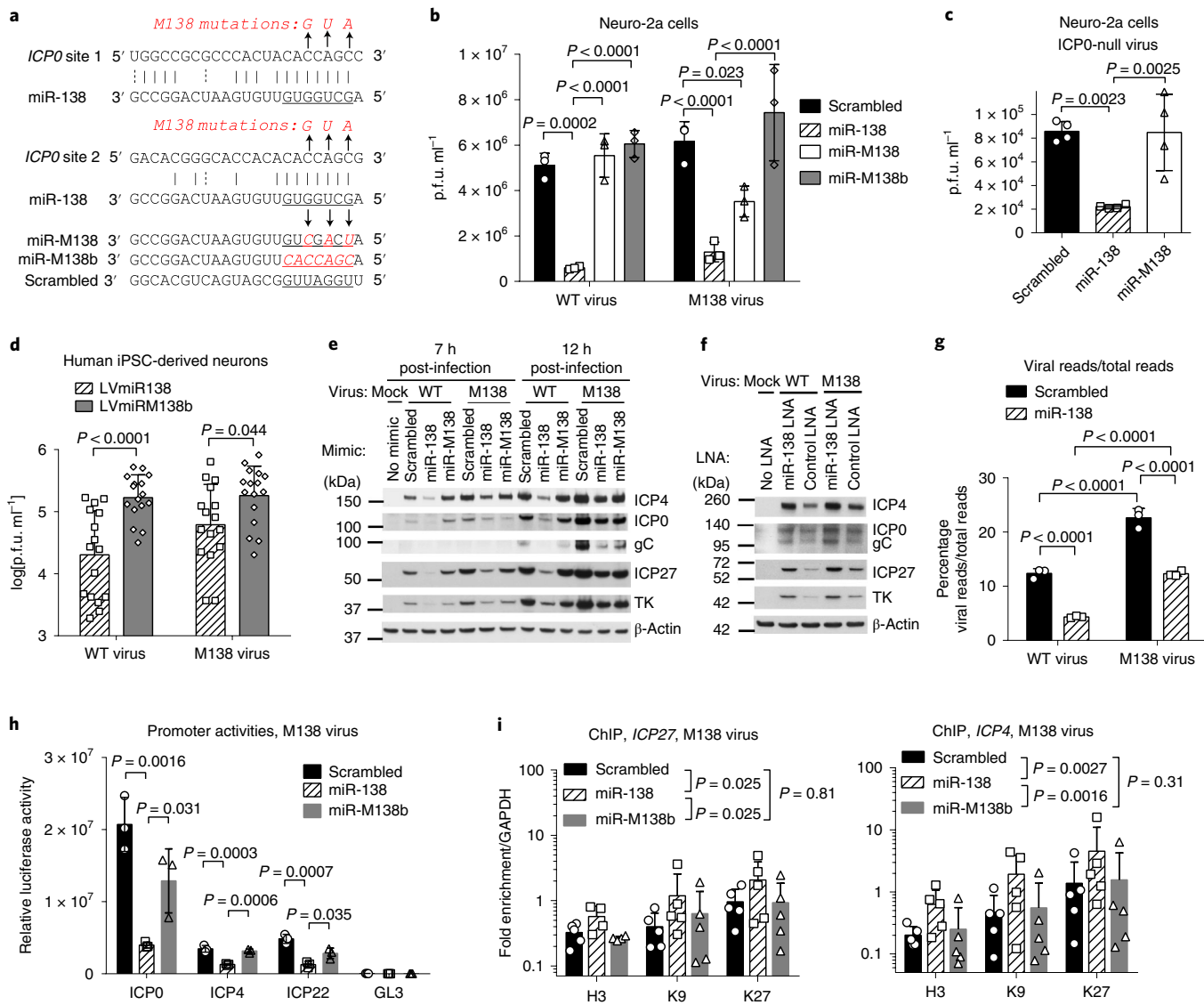


Fig. 1 | ICPO-independent suppression of viral replication by miR-138 in Neuro-2a cells. **a**, Sequences of miR-138, its target sites in the *ICP0* 3'-UTR, the M138 mutations and synthetic miRNA mimics. Seed regions are underlined. The arrows point to the nucleotide substitutions. **b**, Neuro-2a cells were transfected with 10 nM of miRNA mimic for 16 h, then infected at an MOI of 1 for 48 h before viral titre measurements. **c**, Same as **b**, except that 40 nM of miRNA mimic was transfected and cells were infected with 7134 virus (MOI = 5). **d**, Human neurons differentiated from iPSCs were transduced with a lentivirus expressing miR-138 (LVmiR138) or one with the miR-138 seed region mutated to that of miR-M138b (LVmiRM138b), then infected with WT or M138 virus (MOI = 1) for 48 h before viral titre measurements. Data were combined from four independent replicate experiments, each with four biologically independent samples per condition. (The data from each experiment were first normalized to the value from the LVmiRM138b WT virus group before being combined, so $n=16$ biologically independent samples per condition.) **e**, Neuro-2a cells were transfected with 40 nM of miRNA mimic for 16 h, then infected (MOI = 5) for 7 or 12 h before western blot analysis. This experiment was repeated once with similar results. **f**, Neuro-2a cells were transfected with 40 nM of LNA for 8 h, then infected (MOI = 3) for 16 h before western blot analysis. This experiment was repeated three times with similar results. **g**, Neuro-2a cells were transfected with 40 nM of miRNA mimic for 24 h, then infected (MOI = 10) for 16 h before RNA-seq analysis. **h**, Neuro-2a cells were cotransfected with 100 ng ml⁻¹ luciferase plasmid and 16 nM of miRNA mimic for 24 h, then infected (MOI = 1) with M138 virus for 6 h before measuring luciferase activity. **i**, Neuro-2a cells were transfected with 60 nM of miRNA mimic for 24 h, then infected with M138 virus (MOI = 5) for 6 h before ChIP-qPCR analysis of total histone H3 (H3), H3K9me3 (K9) and H3K27me3 (K27) at the *ICP27* and *ICP4* promoters. Log transformations of the means from each of two experiments (a total of five biologically independent samples) were analysed by two-way repeated measures analysis of variance (ANOVA) with Holm–Šídák's multiple comparisons tests for the main effects of the miRNA treatment factor. **b,g,h**, $n=3$ biologically independent samples per condition. **c**, $n=4$ biologically independent samples per condition. **e,f**, Data were analysed by one-way ANOVA with Bonferroni's multiple comparisons tests. **b,g,h**, Data were analysed by two-way ANOVA with Bonferroni's multiple comparisons tests. Data are presented as the mean \pm s.d.

BAC virus²⁸ (designated WT in this article); M138 virus²⁶, which has mutations in the miR-138 binding sites in *ICP0* mRNA (Fig. 1a); and *ICP0*-null mutant virus 7134 (ref. ²⁹). We used 3 control miRNA mimics: a scrambled sequence; miR-M138; and miR-M138b (Fig. 1a). miR-M138 contains mutations complementing the M138 mutations

in *ICP0* mRNA whereas miR-M138b contains a mutant seed region complementary to neither WT *ICP0* nor M138 *ICP0*. Consistent with previous results²⁶, WT and M138 virus yields were similar after transfection with scrambled and miR-M138b controls (Fig. 1b). The viruses did not differ significantly for any effects on expression

of miR-138 (Extended Data Fig. 1a). While transfected miR-138 reduced WT virus yields by almost tenfold compared to the three controls, it also reduced M138 virus yields by approximately four-fold compared to scrambled and miR-M138b controls at 48 h post-infection (Fig. 1b). The effects on WT virus can be partially attributed to the activity of miR-138 against ICP0 because the fold change caused by miR-138 in multiple replicate experiments was on average approximately twofold higher for WT than M138 virus (Extended Data Fig. 1b). Also, miR-M138, which should target the *ICP0* of the M138 virus due to the compensatory mutations, suppressed M138 virus replication by approximately twofold (Fig. 1b). However, ICP0-independent suppression contributed more (four to fivefold) as estimated from the impact of miR-138 on the M138 virus. Moreover, transfected miR-138 reduced *ICP0*-null virus yields in Neuro-2a cells (Fig. 1c). Furthermore, transduction of human neurons derived from induced pluripotent stem cells (iPSCs) with a lentivirus expressing miR-138 significantly reduced replication of both WT and M138 viruses relative to a control lentivirus, with WT virus showing a greater reduction (Fig. 1d). However, in 293T (human embryonic kidney) cells, transfected miR-138 more modestly suppressed replication of WT, M138 and *ICP0*-null viruses (Extended Data Fig. 1c); in Vero cells, transfected miR-138 had little effect on WT and M138 virus (Extended Data Fig. 1d). Overall, we observed cell type-specific effects of miR-138 on HSV-1 replication that were both ICP0-dependent and independent, with greater effects in neuronal cells.

miR-138 regulates viral gene expression and chromatin. To determine the effects on gene expression, we conducted western blot analyses after transfection-infection of Neuro-2a cells. In WT-infected cells, transfected miR-138 reduced the expression of all viral proteins analysed at 7 and/or 12 h post-infection compared to scrambled and miR-M138 controls (Fig. 1e). In M138 virus-infected cells, these proteins were also reduced by miR-138 compared to the scrambled control, indicating ICP0-independent repression. Relative to the scrambled control, miR-M138 also reduced protein expression from the M138 virus, presumably by miR-M138 targeting of mutant *ICP0* mRNA. Importantly, a locked nucleic acid (LNA) inhibitor of miR-138 increased protein expression from both WT and M138 viruses at 16 h post-infection relative to a negative LNA control (Fig. 1f).

We next performed RNA sequencing (RNA-seq) on Neuro-2a cells that had been transfected with miRNA mimics and infected with WT or M138 virus for 16 h. We observed approximately two-fold higher ratios of viral reads/total reads in M138-infected relative to WT-infected cells after transfection with the scrambled mimic, which we ascribe to loss of repression of ICP0 by endogenous miR-138. Relative to the scrambled control, transfected miR-138 reduced the ratios of viral reads/total reads for both WT (approximately 2.8-fold) and M138 (approximately 1.8-fold) viruses (Fig. 1g). Therefore, ICP0-dependent and ICP0-independent mechanisms contributed approximately 1.5 (2.8/1.8) and approximately 1.8-fold repression, respectively. The average read numbers for each viral transcript decreased on miR-138 transfection by 2.3–3.6-fold for WT and 1.5–2.3-fold for M138 virus (Extended Data Fig. 2), with no transcripts being particularly affected.

Given these global effects, we tested the effects of miR-138 on virus gene transcription by cotransfected Neuro-2a cells with an miRNA mimic and one of three plasmids with an immediate-early promoter of the *ICP0*, *ICP4* or *ICP22* gene driving luciferase expression before infection with M138 virus for 6 h. The luciferase activities, which were dramatically induced after infection, were reduced by transfected miR-138 (Fig. 1h). We then examined whether miR-138 affects viral chromatin status. After transfection with miRNA mimics, we infected Neuro-2a cells with M138 virus for 6 h before chromatin immunoprecipitation (ChIP). Compared to both scrambled and miR-M138b controls, transfected miR-138 increased the

association of total histone H3, as well as H3K9me3 and H3K27me3 modifications with *ICP27* and *ICP4* promoters (Fig. 1i). Together, miR-138 globally represses lytic gene expression, independent of ICP0, at least in part by a mechanism that increases heterochromatin on viral genes.

miR-138 reduces lytic gene expression in murine ganglia. To investigate this repression *in vivo*, we used a previously described virus, WT^{Lyt138}, here named WT^{miR138}, with miR-138-expressing sequences inserted between the *US11* and *US12* coding regions in the WT virus³⁰. We also constructed a virus with the same insertion in the M138 background, designated as M138^{miR138} (Fig. 2a). Control viruses with the same insertion but a mutated seed region were also constructed and designated WT^{nomiR138} or M138^{nomiR138}. Northern blot hybridization showed no detectable expression of the mutated miRNA (Extended Data Fig. 3a). We also restored the WT seed sequence to these nomiR138 viruses to result in a second pair of independently constructed miR-138-expressing viruses named WT^{miR138R} or M138^{miR138R}. All six recombinant viruses expressed WT levels of *US11* or *US12* mRNA in Vero cells (Extended Data Fig. 3b). All four miR-138-expressing viruses significantly increased miR-138 levels in both Neuro-2a and 293T cells (Fig. 2b and Extended Data Fig. 3c).

We next infected mice with these viruses at the cornea. Pairwise comparisons showed similar viral genome levels but significantly decreased lytic transcript (*ICP0*, *TK* and *gC*) levels from the miR-138-expressing viruses (WT^{miR138} and WT^{miR138R}) relative to the control virus (WT^{nomiR138}) in trigeminal ganglia at 5 days post-infection (Extended Data Fig. 4a,b). We next examined the M138-derived viruses to assess whether the effects depended on ICP0. The three viruses showed similar eye swab titres at 1 d post-infection (Fig. 2c). At 5 d post-infection, the two miR-138-expressing viruses, M138^{miR138} and M138^{miR138R}, both showed lower levels of *ICP0*, *TK* and *gC* transcripts (normalized to genome levels) than the control virus, M138^{nomiR138}, with all but one of the differences being statistically significant (Fig. 2d and Extended Data Fig. 4c). Thus, ectopically expressed miR-138 can repress viral gene expression independent of ICP0 in acutely infected mouse ganglia.

***ICP0* is the only confirmed HSV-1 target of miR-138.** To understand ICP0-independent repression, we first looked for other viral targets by photoactivatable ribonucleoside-enhanced cross-linking and immunoprecipitation (PAR-CLIP). We constructed 293T138 and 293Tcontrol cells by transducing 293T cells with miR-138-expressing and empty lentiviruses, respectively. 293T138 cells expressed 500-fold more miR-138 than 293Tcontrol cells (Extended Data Fig. 5a). After a PAR-CLIP experiment that compared 293T138 and 293Tcontrol cells (Extended Data Fig. 5b), we found >100-fold more miR-138 reads in AGO immunoprecipitates from 293T138 than 293Tcontrol cells at both 4 and 8 h post-infection (Extended Data Fig. 5c). Of 22 viral mRNA sequences complementary to the miR-138 seed sequence (GCUGGUG), besides the two sites in the *ICP0* 3'-UTR, only one site in the *UL39* coding sequence (CDS) fulfilled our criteria (>20 reads in 293T138 cells and greater than twofold more reads in 293T138 than 293Tcontrol cells) at one or both time points (Extended Data Fig. 5c). However, transfected miR-138, which decreased ICP0 expression from an ICP0-expressing plasmid, did not decrease UL39 expression from a UL39-expressing plasmid (Extended Data Fig. 5d). Thus, *ICP0* mRNA was the only viral target of miR-138 that we could confirm.

Identification of *Oct-1* and *Foxc1* as targets of miR-138. We next searched for host targets of miR-138. Human transcripts were analysed using the PAR-CLIP data from 293Tcontrol and 293T138 cells that had been infected for 4 h. To identify host targets in neuronal

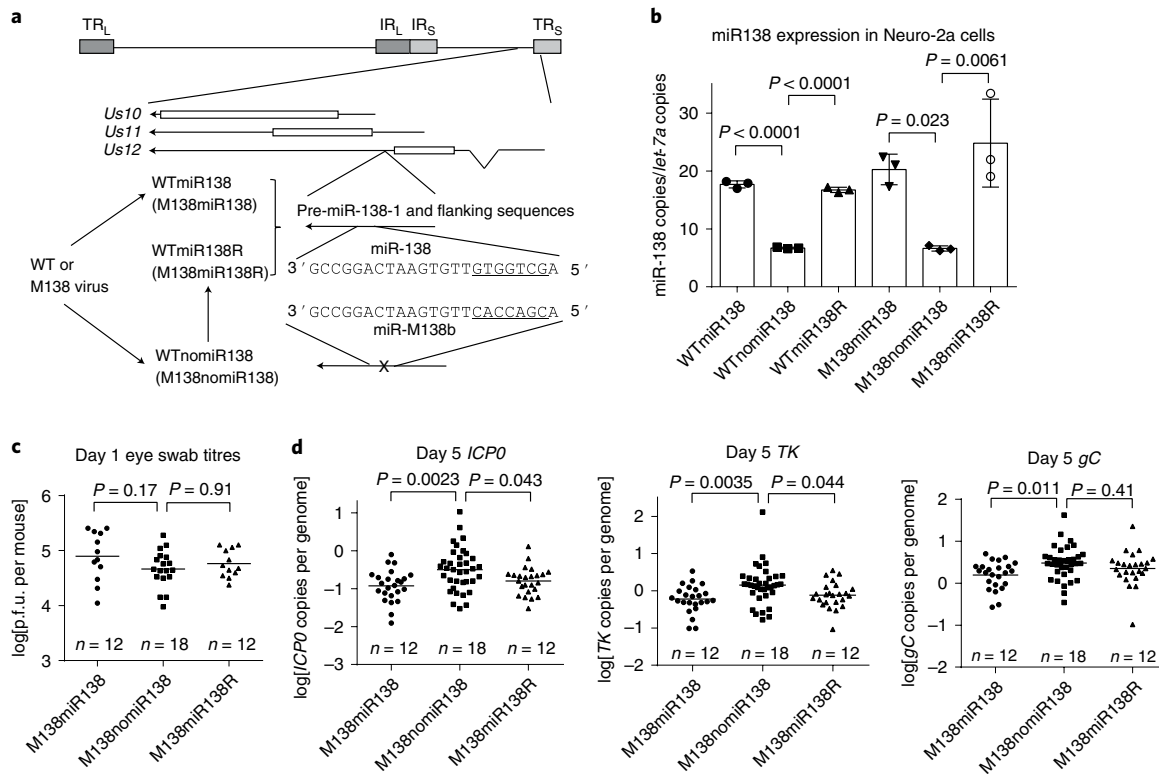


Fig. 2 | miR-138 reduces viral gene expression in acutely infected mouse trigeminal ganglia. a, Genomic location of inserted miR-138-expressing sequences. The HSV-1 genome is depicted as a horizontal line at the top with long (TR_L and IR_L) and short (IR_S and TR_S) repeat sequences shown as grey boxes. Below, the insertion location is expanded, with the bars representing the CDS and the arrows representing mRNAs. The inserted sequences are further expanded to show miR-138 and miR-M138b sequences (seed regions are underlined) that correspond to the recombinant viruses shown to the left. The order of virus derivation is indicated by arrows connecting the virus names. **b,** miR-138 expression (relative to *let-7a* expression) from Neuro-2a cells infected by the indicated recombinant viruses (8 h post-infection, MOI=10) as measured by qPCR with reverse transcription (RT-qPCR). *n*=3 biologically independent samples per condition. Data are presented as the mean \pm s.d. **c,d,** Viral titres in eye swabs at 1 d post-infection after corneal inoculation of mice with 2×10^5 p.f.u. per eye of the indicated viruses. **d,** Viral transcript levels (as measured by RT-qPCR) normalized to viral genome levels (as determined by qPCR) in trigeminal ganglia at 5 d post-infection with the indicated viruses. **c,d,** Each point represents a value from one mouse (**c**) or trigeminal ganglion (**d**), the horizontal lines represent the geometric means and the numbers of mice used (*n*) are displayed above the horizontal axes. **b,c,d,** Data were analysed by one-way ANOVA with Bonferroni's multiple comparisons.

cells, we derived N2A138 cells from Neuro-2a cells that expressed fivefold more miR-138 than Neuro-2a cells using the same method as for 293T138 cells (Extended Data Fig. 5e). Considering the high endogenous expression of miR-138 in Neuro-2a cells, we also constructed N2Aanti138 cells using lentivirus expressing ‘tough decoy’ antisense sequences (Extended Data Fig. 5f)³¹. We then performed a PAR-CLIP experiment comparing uninfected N2A138 and N2Aanti138 cells. In the PAR-CLIP data, miR-138 reads were approximately fivefold higher in N2A138 than N2Aanti138 cells (Extended Data Fig. 5g). For PAR-CLIP data from cell lines derived from both 293T and Neuro-2a cells, counts of canonical seed-matching reads aligned to the 5'-UTR, CDS and 3'-UTR of each transcript were calculated separately. After applying criteria for both read counts and fold differences (Fig. 3a), we identified 5, 176 and 121 transcripts with sites in 5'-UTRs, CDS and 3'-UTRs, respectively in 293T cells, and 4, 200 and 111 transcripts with sites in these regions, respectively in Neuro-2a cells (Fig. 3b).

We next combined PAR-CLIP and RNA-seq to detect transcripts that both bind to miR-138 and exhibit reduced abundance in its presence. RNA-seq analyses showed that relative to the scrambled control, transfected miR-138 significantly ($P < 0.01$) reduced levels of 266 and 270 transcripts in 293T and Neuro-2a cells, respectively by \log_2 decreases >0.5 (Fig. 3a,b). Comparisons of the PAR-CLIP and RNA-seq results resulted in 1, 15 and 22 transcripts identified

in both assays with sites in 5'-UTRs, CDS and 3'-UTRs, respectively in 293T cells, and 0, 11 and 23 transcripts with sites in these regions, respectively in Neuro-2a cells. Relative to the single PAR-CLIP approach, the combined approach identified significantly higher fractions of targets with 3'-UTR sites (Extended Data Fig. 5h).

In the final PAR-CLIP/RNA-seq results, six transcripts (list A, Fig. 3c) were identified in both 293T and Neuro-2a cells, namely *Bcl9*, *Pou2f1* and *Rere* with CDS sites, and *Foxc1*, *Rara* and *Tpm4* with 3'-UTR sites. Being particularly interested in neuronal cells, we applied more stringent criteria (\log_2 fold change >0.8) to targets with 3'-UTR sites identified only in Neuro-2a cells to form list B (Fig. 3c). Combining lists A and B yielded 17 transcripts (Fig. 3c and Supplementary Table 1). For each of them, we designed short interfering RNAs (siRNAs) and selected the most effective one. The expression of each gene other than *Nova2* was reduced by 50–95% by the selected siRNA as assessed by western blotting (Fig. 3d) and/or RT-qPCR (Extended Data Table 2). We then infected siRNA-transfected Neuro-2a cells with WT virus. Compared to two control siRNAs, siRNAs against *Ccdc6*, *Daam2*, *Pou2f1* and *Foxc1* significantly reduced viral yields (Fig. 3e). We focused on *Pou2f1* and *Foxc1* in the following experiments because their siRNAs had the greatest effects. Interestingly, they are both transcription factors and *Pou2f1* encodes the aforementioned cofactor of VP16, OCT-1.

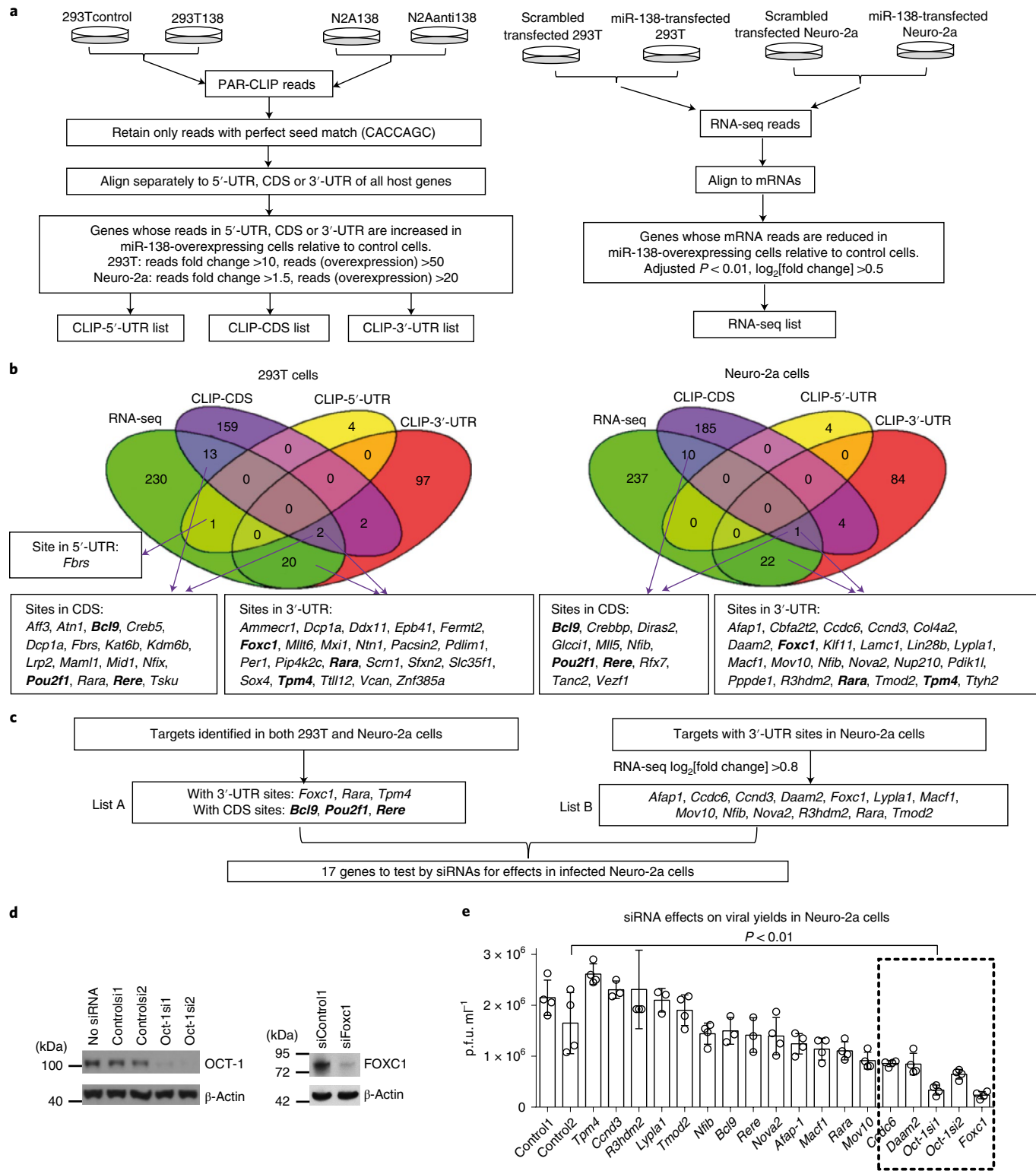


Fig. 3 | Host targets of miR-138 identified by PAR-CLIP/RNA-seq/siRNA screening. **a**, Outline of the procedures used to perform and analyse PAR-CLIP and RNA-seq. **b**, Venn diagrams generated using the lists obtained in **a**. The four boxes just below the Venn diagrams show the lists of genes found in both the RNA-seq list and the CLIP-CDS, CLIP-5'-UTR or CLIP-3'-UTR list. The purple arrows point from the locations of the genes in the Venn diagrams to those in the boxes. Genes found in both 293T and Neuro-2a cells are shown in bold. **c**, Criteria for further selection of genes for the siRNA experiments. **d**, Neuro-2a cells were transfected with 80 nM of the indicated siRNA and collected at 48 h post-infection for western blot analysis of OCT-1-1 (left), FOXC1 (right) and β-actin (both). These experiments were repeated once with similar results. **e**, Neuro-2a cells were transfected with 80 nM of the siRNAs against the indicated genes for 48 h, then infected with WT virus (MOI = 0.1) for 48 h before viral titre measurements. $n = 3$ or 4 biologically independent samples per condition. Data are presented as the mean values \pm s.d. The box with the dashed outline indicates siRNAs that reduced viral titres significantly relative to Control2 siRNA ($P < 0.01$, one-way ANOVA with Bonferroni's multiple comparisons tests).

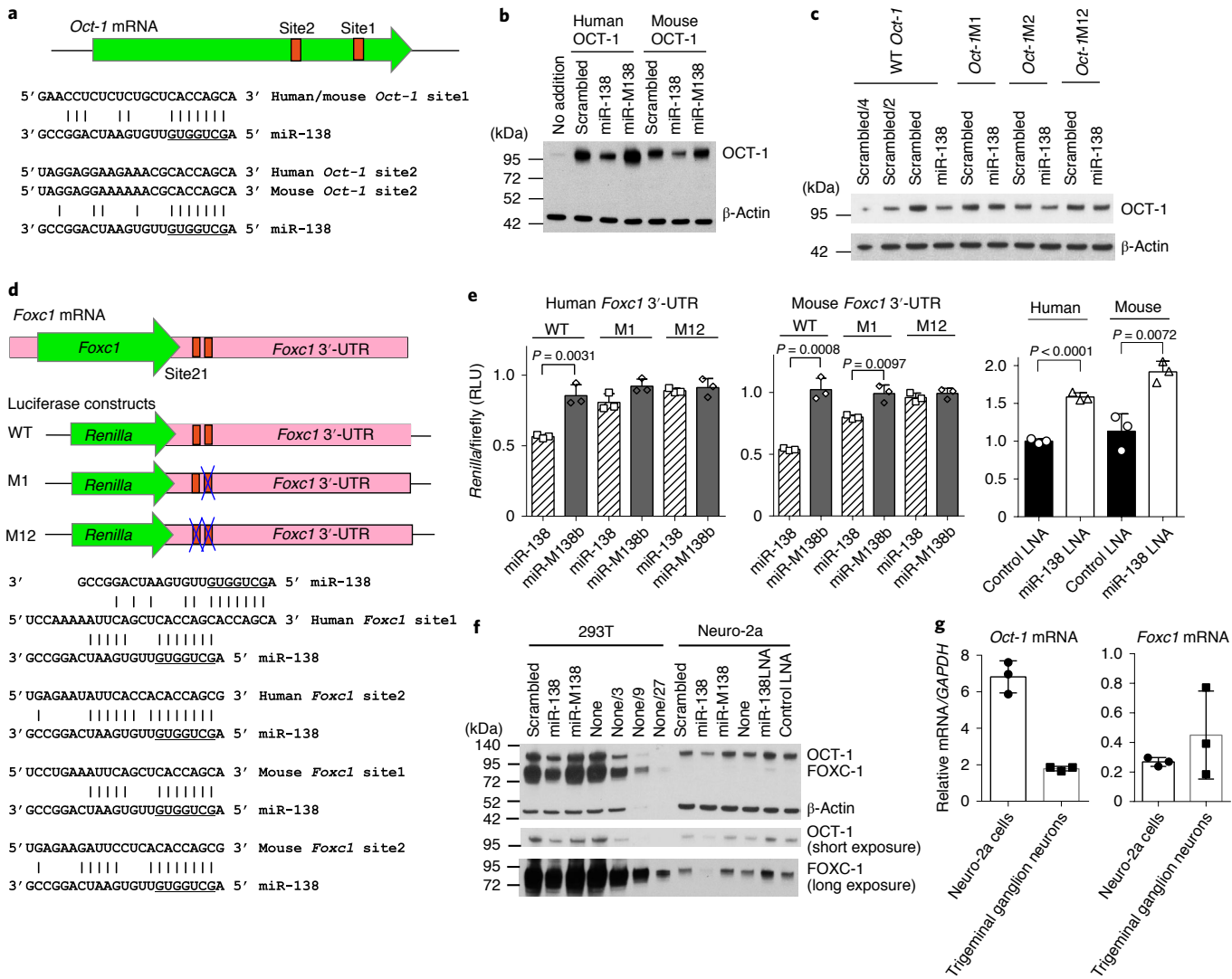


Fig. 4 | Repression of *Oct-1* and *Foxc1* expression by miR-138. **a**, miR-138 binding sites in the *Oct-1* CDS. The horizontal line represents *Oct-1* mRNA. The thick green arrow represents the *Oct-1* CDS. The two small orange boxes represent miR-138 binding sites, whose sequences and how they pair with miR-138 (seed region underlined) are shown. **b**, 40 nM of miRNA mimic and 100 ng ml⁻¹ of *Oct-1*-expressing plasmid were cotransfected into 293T cells for 30 h before western blot analysis. This experiment was repeated twice with similar results. **c**, Same as **b**, but using plasmids expressing WT human *Oct-1* or its variants with mutations at site1 (M1), site2 (M2) or both sites (M12). This experiment was repeated once with similar results. **d**, *Foxc1* mRNA and luciferase constructs are illustrated with the pink horizontal bar representing *Foxc1* mRNA and the embedded green arrow representing *Foxc1* CDS. The two small orange boxes represent miR-138 binding sites, whose sequences and how they pair with miR-138 (seed region underlined) are shown. Blue X's indicate mutated sites. **e**, Left and middle, 293T cells were cotransfected with 40 nM of miRNA mimic and 100 ng ml⁻¹ of plasmid and collected at 48 h for assay of luciferase activity. Right, 293T cells were cotransfected with 20 nM of miR-138 mimic, 20 nM of miR-138 or control LNA and 40 ng ml⁻¹ of luciferase plasmid with human or mouse *Foxc1* 3'-UTR before being collected at 48 h for assay of luciferase activity. RLU, relative luciferase unit. Data were analysed by two-tailed, unpaired t-tests. **f**, 293T or Neuro-2a cells were transfected with 80 nM of miRNA mimic or 20 nM of LNA and collected for western blot analysis at 72 h after transfection. Dilutions of lysates of non-transfected cells are indicated as none, none/3, etc. This experiment was repeated once with similar results. **g**, *Oct-1* and *Foxc1* mRNA levels in Neuro-2a cells and neurons purified from mouse trigeminal ganglia were analysed by RT-qPCR. **e,g**, *n*=3 biologically independent samples per condition; data are presented as mean values±s.d.

miR-138 represses *Oct-1* and *Foxc1*. The *Oct-1* CDS has two canonical (perfect seed matching) sites (Fig. 4a). Both are conserved between humans and mice and belong to the 8mer type, a target site type with the highest efficacy¹. After cotransfection with OCT-1-expressing plasmids, miR-138 repressed expression of human and mouse OCT-1 (Fig. 4b). The effect on human OCT-1, which was approximately twofold for WT, was less when either site alone was mutated and largely eliminated when both sites were mutated (Fig. 4c), suggesting that miR-138 represses *Oct-1* through these sites.

Both human and mouse *Foxc1* have two canonical sites in their 3'-UTRs; unusually, site1 in human but not mouse *Foxc1* can bind miR-138 in two ways (Fig. 4d). After cotransfection with luciferase constructs, miR-138 repressed luciferase activity from mRNAs with human and mouse *Foxc1* 3'-UTRs; repression was alleviated by cotransfection with an LNA inhibitor (Fig. 4e). For both human and mouse *Foxc1* 3'-UTRs, repression was greatly attenuated when site1 was mutated and obliterated when both sites were mutated, suggesting that miR-138 represses *Foxc1* through both sites.

We then examined regulation of endogenous OCT-1 and FOXC1 expression by miR-138. Transfected miR-138 reduced FOXC1 and OCT-1 expression by approximately threefold and twofold, respectively in 293T and Neuro-2a cells (Fig. 4f). A transfected miR-138 LNA inhibitor increased FOXC1 (approximately twofold) and OCT-1 (less than twofold) expression in Neuro-2a cells (Fig. 4f). Relative to 293T cells, Neuro-2a cells exhibited greater than threefold lower OCT-1 and >27-fold lower FOXC1 protein levels (Fig. 4f). Relative to Neuro-2a cells, neurons isolated from mouse trigeminal ganglia exhibited approximately fourfold lower *Oct-1* and similar *Foxc1* mRNA levels (Fig. 4g). Data from a database (<http://mousebrain.org/>) also showed low, albeit detectable *Oct-1* and *Foxc1* mRNA levels in ganglionic neurons. Moreover, immunofluorescence assays showed that although trigeminal ganglion cryosections displayed strong signals when stained with a neuronal marker Tuj1, neither OCT-1 nor FOXC1 was detected meaningfully above background in cells expressing Tuj1 using validated antibodies (Extended Data Fig. 6). Thus, OCT-1 and FOXC1 are expressed poorly in ganglionic neurons, the site of HSV-1 latency, correlating with high miR-138 expression in such neurons^{20,26}.

FOXC1 increases HSV-1 replication in neurons. Unlike OCT-1, FOXC1 was not known to regulate HSV-1 infection. FOXC1 contains a DNA-binding domain (DBD), an N-terminal activation domain (AD-N), a C-terminal activation domain (AD-C) and an inhibitory domain (ID)^{32,33} (Fig. 5a). Compared to an empty vector (pcDNA), transfected human or mouse FOXC1 greatly increased virus replication in Neuro-2a cells (Fig. 5b,c). The human FOXC1 mutant without the DBD no longer promoted viral replication (Fig. 5c). Deletion of either AD attenuated FOXC1's ability to promote viral replication, but deletion of both (delADboth) resulted in viral yields even lower than those exhibited by pcDNA, which is suggestive of dominant-negative effects (Fig. 5c). Interestingly, deletion of the ID (delID) resulted in viral yields even higher than the increased yields exhibited by full-length FOXC1 (Fig. 5c). Thus, stimulation of HSV-1 replication by FOXC1 requires DNA binding and is positively regulated via the ADs and negatively regulated via the ID. We then transduced cultured neurons isolated from mouse trigeminal ganglia with adeno-associated virus (AAV) expressing FOXC1, FOXC1delADboth or FOXC1delID before infection with an HSV-1-expressing green fluorescent protein (HSV1GFP). Immunofluorescence analysis confirmed efficient transduction of almost all neurons and indicated higher GFP expression from HSV1GFP in AAVFOXC1 than AAVFOXC1delAD-transduced neurons (Fig. 5d). Relative to AAVFOXC1delAD, transduction of AAVFOXC1 resulted in higher HSV1GFP titres in supernatants at 72 h post-infection (Fig. 5e). We also observed higher HSV1GFP titres in supernatants over AAVFOXC1delID than AAVFOXC1delAD-transduced neurons at 24 and 60 h post-infection (Fig. 5f).

Fig. 5 | FOXC1 promotes HSV-1 replication in neuronal cells and mouse trigeminal ganglia. **a**, Schematics of full-length human FOXC1 and its deletion mutants. The positions of the ADs, DBD and ID are shown. **b**, Neuro-2a cells were transfected with 200 ng ml⁻¹ of plasmid for 24 h before western blot analysis. This experiment was repeated once with similar results. **c**, Neuro-2a cells were transfected with 200 ng ml⁻¹ of plasmid for 24 h, then infected with the KOS strain (MOI = 0.1) for 48 h before viral titre measurements. **d**, Neurons were isolated from mouse trigeminal ganglia, cultured and transduced with the indicated AAV for 5 d before infection with HSV1GFP (MOI = 2). At 72 h post-infection, they were fixed and stained with anti-FLAG antibody to detect FLAG-tagged FOXC1 and FOXC1delAD proteins (blue) and with anti-Tuj1 (red) antibodies. This experiment was repeated twice with similar results. **e**, In the experiment described in **d**, supernatants were collected for viral titre measurements. **f**, Same as **e** except that an MOI of 10, different AAVs and time points were used, as indicated. **g**, Schematic of recombinant viruses showing the location of insertion. **h**, After corneal inoculation of mice with 4 × 10⁴ p.f.u. per eye, eye swab viral titres were measured. **i**, After inoculation as in **h**, mouse trigeminal ganglia collected at 3 d post-infection were analysed for viral titres. **j**, Eighteen days after inoculation with 2 × 10⁵ p.f.u. per eye, the severity of mouse facial lesions was scored: 0, no lesion; 1, slight lesions in small areas; 2, nearly half of the face covered by lesions; 3, most of the face covered by lesions. Data were analysed by two-tailed, paired (**h**) or unpaired (**i**) t-tests, or one-way (**c,j**) or two-way (**e,f**) ANOVA with Bonferroni's multiple comparisons tests. **c,e,f**, Each point represents a biologically independent sample ($n=3-8$). **h,i,j**, Each point represents one mouse (**h,j**) or trigeminal ganglion (**i**). The number of mice used is indicated as n . **e,f**, Data are presented as mean values ± s.d. **c,h,i**, The horizontal lines represent geometric means.

To further investigate FOXC1 effects in mice, we constructed a recombinant virus expressing FOXC1, designated HSV1FOXC1 (Fig. 5g). For unknown reasons, HSV1FOXC1 showed a one-log defect in ocular replication relative to WT 1 d after corneal inoculation (Extended Data Fig. 7a). Consequently, HSV1FOXC1 also showed significantly lower viral genome levels at 31 d post-infection (Extended Data Fig. 7b). (Similarly low mortality, <5%, was observed for both viruses.) Despite decreased replication in the eye probably influencing the amounts of virus entering the trigeminal ganglion, HSV1FOXC1 titres were similar to WT titres in the trigeminal ganglion at 5 d post-infection (Extended Data Fig. 7c) hinting at possible increased replication in neuronal tissues. We then constructed another control virus designated as HSV1FOXC1delAD expressing FOXC1delADboth. Expression of FOXC1 and FOXC1delAD proteins from these viruses in trigeminal ganglia at 3 d post-infection was confirmed by immunofluorescence (Extended Data Fig. 7d). Despite similar eye swab titres at 1 and 3 d post-infection (Fig. 5h), HSV1FOXC1 replicated to significantly higher titres than HSV1FOXC1delAD in trigeminal ganglia at 3 d post-infection (Fig. 5i). Also, from 3 to 5 d post-infection, the eye swab titres of HSV1FOXC1 increased significantly while the HSV1FOXC1delAD titres were unchanged (Fig. 5h). To rule out the possibility that the lower replication of HSV1FOXC1delAD was due to unwanted mutations, we independently engineered another FOXC1delADboth-expressing virus named HSV1FOXC1delADb, which also showed significantly lower titres in trigeminal ganglia at 3 d post-infection than HSV1FOXC1 (Fig. 5i). At 29 d post-infection, when latency was fully established, we did not detect a difference in viral genome levels between HSV1FOXC1, HSV1FOXC1delAD and HSV1FOXC1delADb (Extended Data Fig. 7e). However, we observed significantly more severe facial lesions caused by HSV1FOXC1 than either HSV1FOXC1delAD or HSV1FOXC1delADb at 18 d post-infection (Fig. 5j). Thus, FOXC1 can promote HSV-1 replication in neuronal cells in culture and nervous tissues *in vivo* and affect viral pathogenesis.

FOXC1 upregulates HSV-1 gene expression. To understand how FOXC1 promotes HSV-1 replication, we first analysed gene expression in Neuro-2a cells. All viral proteins tested were upregulated by FOXC1 with effects observed as early as 4 h post-infection (Fig. 6a). Even at 2 h post-infection, all viral transcripts tested were significantly upregulated by FOXC1delID relative to FOXC1delAD (Fig. 6b and Extended Data Fig. 8a). However, attachment to cells and entry of viral genome into the nucleus (Fig. 6c) were not affected, demonstrating that FOXC1 promotes transcription rather than upstream steps. RNA-seq analysis comparing pFOXC1human- and pcDNA-transfected Neuro-2a cells showed that at 5 h post-infection all viral transcripts were upregulated by FOXC1 without any one being particularly more so than others (Extended Data Fig. 8b). However, immediate-early transcripts were generally

less upregulated possibly because of their high baseline levels resulting from activation by the VP16–OCT-1–HCF-1 complex.

FOXC1 is important for miR-138 regulation of HSV-1. We derived a FOXC1 knockout cell line from Neuro-2a cells using CRISPR–Cas9 technology (Extended Data Fig. 9a). These cells

showed substantially reduced viral replication and viral protein and mRNA levels at early times (Fig. 6d,e and Extended Data Fig. 9b,c). Transfection of FOXC1 into N2AFOXC1 knockout cells increased viral mRNA levels roughly to those observed in Neuro-2a cells transfected with empty vector, indicating that the loss of FOXC1 is responsible for reduced viral replication (Fig. 6e and Extended Data

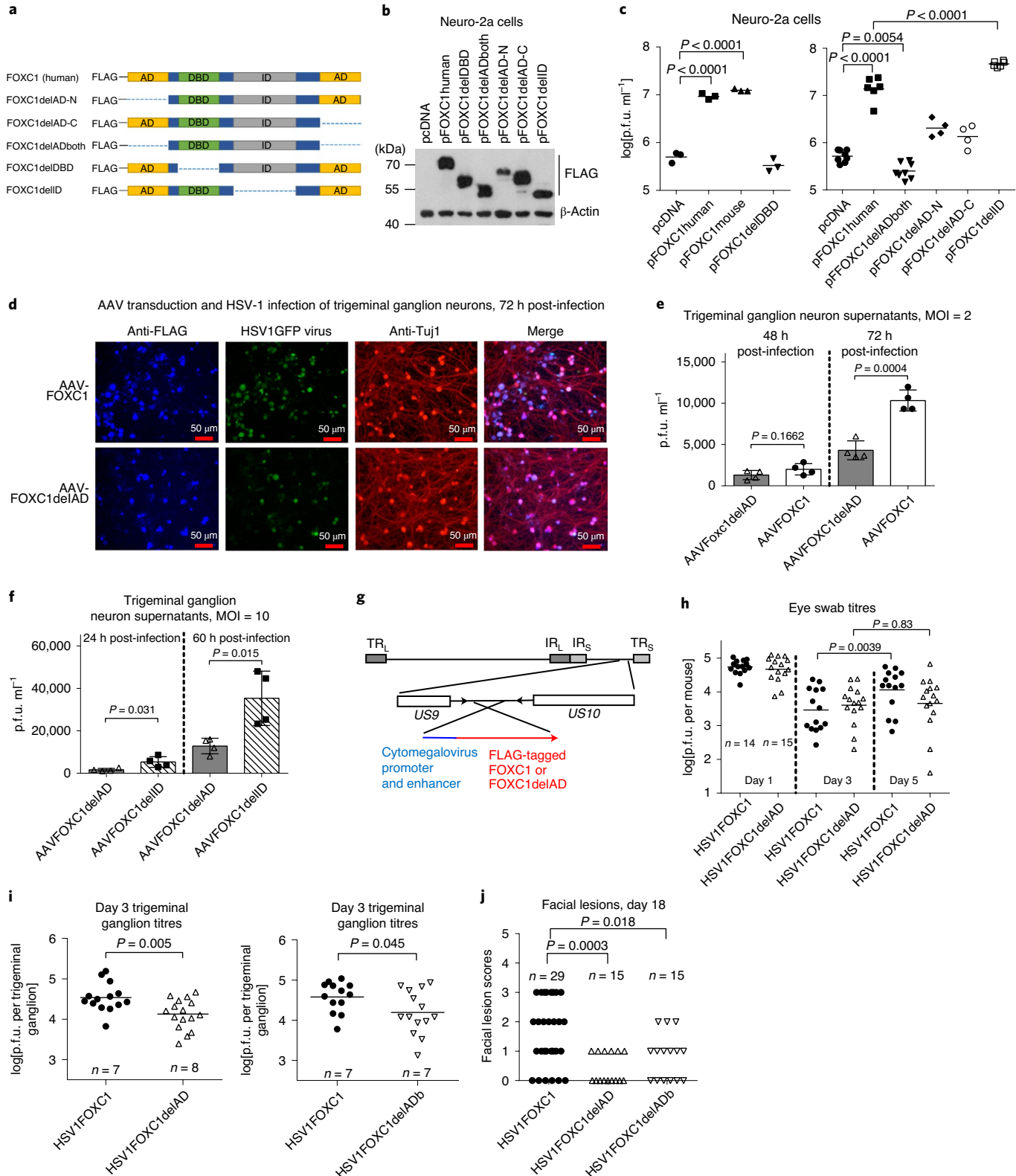


Fig. 9c). Notably, miR-138 repression of viral replication was markedly attenuated in N2AFOXC1 knockout cells (Fig. 6f). Thus, even though its expression was already low in neuronal cells (Fig. 4f,g), FOXC1 was important for viral replication and gene expression and their repression by miR-138.

Heterochromatin reduction by FOXC1 and ICP0. The global effects of FOXC1 on viral transcription prompted us to investigate whether FOXC1 modulates viral chromatin status. The ChIP with qPCR (ChIP-qPCR) experiments showed that transfected full-length FOXC1 reduced H3K9me3 enrichment on *ICP0*, *ICP27* and *ICP8* promoters in KOS virus-infected Neuro-2a cells at 2 h post-infection (Extended Data Fig. 10). To detect the differences more sensitively, we used the plasmid expressing the FOXC1delID mutant, which is more active than full-length FOXC1 (Fig. 5c). Consistent with previous results from fibroblasts¹¹, the histone H3 and H3K9me3 association with the *ICP4*, *ICP27* and *ICP8* promoters dropped from 2 to 5 h post-infection in KOS- but not 7134 (*ICP0*-null) virus-infected Neuro-2a cells. At both times, FOXC1delID markedly reduced H3 and H3K9me3 association with these regions for both viruses (Fig. 6g). Given these results showing heterochromatin reduction by both FOXC1 and ICP0, we wondered whether FOXC1 could compensate for lack of ICP0. Indeed, transfected FOXC1 increased 7134 virus yields despite little effect on the rescued virus, 7134R, after infection of Neuro-2a cells at a high multiplicity of infection (MOI) (Fig. 6h, left). Strikingly, at a low MOI, transfected FOXC1 increased 7134 virus yields by over 500-fold at 48 h post-infection, such that they were greater than those of 7134R after transfection of pcDNA (Fig. 6h, right). Thus, FOXC1 can replace ICP0 to induce removal of heterochromatin and promote viral replication and can further boost both processes in collaboration with ICP0.

Discussion

After observing ICP0-independent repression of lytic gene expression by miR-138, we performed a genome-wide search for other targets of miR-138, leading to the identification of *Oct-1* and *Foxc1* mRNAs. Despite possibly missing false-negative candidates, the final lists of targets from the combined approach are highly likely to be valid since they fulfilled both binding (PAR-CLIP) and functional (RNA-seq) criteria. Indeed, many of the targets with 3'-UTR sites have been previously validated, including *Ccnd3* (ref. ³⁴), *Ferm1*³⁵, *Foxc1* (refs. ^{36–38}), *Lypla1* (ref. ³⁹), *Rara*⁴⁰ and *Sox4* (ref. ⁴¹). Our approach also identified previously unknown targets with CDS sites, which were neglected by target searches focusing on 3'-UTR sites. Therefore, our PAR-CLIP/RNA-seq method complements computational prediction to facilitate discovery of important miRNA targets.

FOXC1 is a forkhead box (FOX) transcription factor with roles in development and disease^{32,42}. Our results indicate that FOXC1 broadly alters the epigenetic status of the HSV-1 genome. One possibility is that FOXC1 regulates chromatin modulatory proteins that in turn regulate HSV-1 infection. An interesting alternative is that FOXC1 affects the histones associated with viral genes. Another FOX protein, FOXA1, is known as a pioneer factor that can open up condensed chromatin by displacing linker histones⁴³. Although the exact mechanism of FOXC1 regulation of HSV-1 infection remains to be elucidated, this study raises the intriguing possibility that some FOX proteins regulate HSV-1 infection by unusual mechanisms.

There have been studies reporting regulation of viral infection by host miRNAs^{44–50}. However, we are unaware of any that describe convergent repression of both viral and host targets. Since miRNAs typically have a modest impact through each interaction with a transcript, they may require multiple interactions to achieve robust outcomes¹. Remarkably, the three targets of miR-138, ICP0, OCT-1 and FOXC1 all play roles in the activation of lytic gene expression and modulation of the viral chromatin status. While ICP0 uses its E3 ubiquitin ligase function, OCT-1 and FOXC1 use their DNA-binding activities. While ICP0 and FOXC1 appear to act globally, OCT-1 acts specifically at immediate-early promoters^{8,9,14}. Targeting these proteins simultaneously blocks multiple paths leading to lytic replication. Both ICP0 and VP16 are crucial for reactivation from latency^{25,51,52}. However, VP16 has little DNA-binding activity on its own⁵³ and has been proposed to act as a switch that can be turned on and off in response to OCT-1 and HCF-1 availability⁸. For example, HCF-1 is sequestered in the cytoplasm of unstimulated neurons, but relocates to the nucleus on reactivation^{54,55}. Low OCT-1 expression in neurons may favour latency by switching VP16 off. Likewise, low expression of FOXC1 that can promote viral replication should also be conducive to latency. Thus, we propose a model where miR-138 expressed highly in neurons promotes latency through multiple convergent pathways involving suppression of these viral and host gene activators (Fig. 6i).

Mammalian alphaherpesviruses, which form latent infections in neurons of species that diverged millions of years ago, use homologues of VP16 to activate gene expression through interaction with OCT-1 (for example, ref. ⁵⁶). We speculate that these viruses evolved neuronal latency by gaining selective advantage from a broad regulatory network, including miR-138, which represses OCT-1 and other factors such as FOXC1. We assume that this network ordinarily helps maintain neuronal identity and function. HSV-1 would then have further evolved to exploit miR-138 for repression of ICP0. It would make sense for evolution to have selected for mechanisms that collaborate rather than offset each other. It will be interesting to see whether such convergent targeting mechanisms are generally exploited by viruses that have evolved to utilize miRNAs.

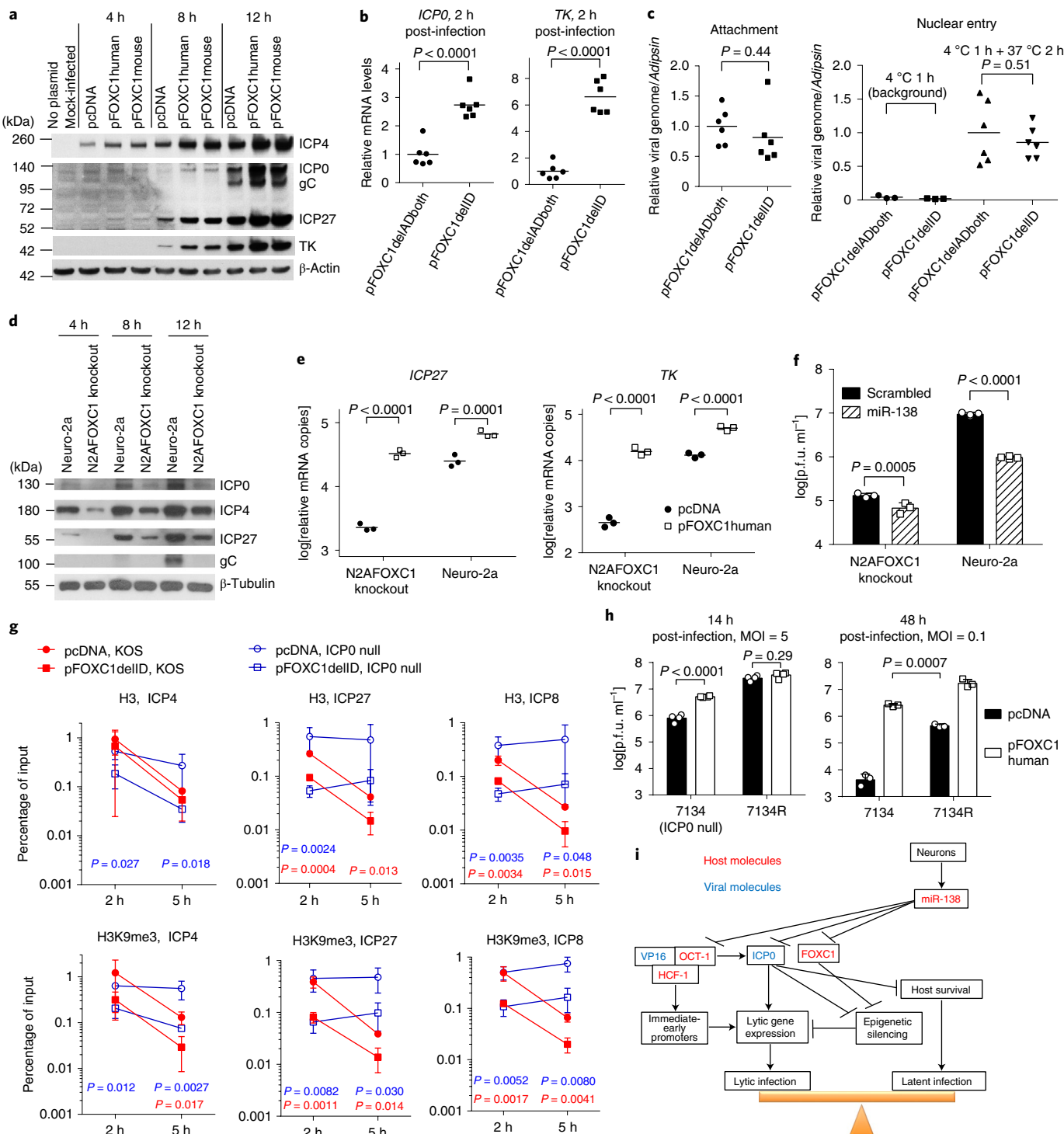
Fig. 6 | FOXC1 effects on HSV-1 gene expression and heterochromatin in Neuro-2a cells. **a**, Neuro-2a cells were transfected with 200 ng ml⁻¹ of plasmid for 24 h, then infected with the KOS strain (MOI = 5) before western blot analysis. **b**, Neuro-2a cells were transfected with 200 ng ml⁻¹ of plasmid for 40 h, then incubated with the KOS strain (MOI = 2) at 4 °C for 1 h to allow attachment, followed by incubation at 37 °C for 2 h before RT-qPCR analysis of RNA levels. **c**, To analyse attachment (left), after transfection and attachment as in **b**, cells were washed before qPCR analysis of viral genome. To analyse nuclear entry (right), after incubation at 37 °C for 2 h (or immediately after attachment to determine the background), nuclear fractions were isolated and analysed by qPCR for viral genome. **d**, Neuro-2a or N2AFOXC1 knockout cells were infected with the KOS strain (MOI = 5) before western blot analysis. **e**, N2AFOXC1 knockout or Neuro-2a cells were transfected with 400 ng ml⁻¹ plasmid, then infected with the KOS strain for 5 h (MOI = 1) before RT-qPCR analyses. **f**, Neuro-2a or N2AFOXC1 knockout cells were transfected with 20 nM of miRNA mimic and infected with the KOS strain (MOI = 0.5) for 48 h before titre measurements. **g**, Neuro-2a cells were transfected with 500 ng ml⁻¹ of plasmid for 40 h and infected with the KOS strain or 7134 virus (MOI = 2) before ChIP-qPCR analysis for histone H3 and H3K9me3 at the indicated promoters; log-transformed data were analysed by multiple t-tests with correction for multiple comparisons using the Holm–Šídák method. When differences between pcDNA and pFOXC1delID are significant, P values are displayed under the points being compared (red for KOS and blue for 7134). **h**, Neuro-2a cells were transfected with 200 ng ml⁻¹ of plasmid, then infected for 14 (MOI = 5, left) or 48 h (MOI = 0.1, right) before viral titre analyses. **i**, Model of regulation of the lytic-latent switch by the neuron-specific miR-138. **b,c**, n = 6 biologically independent samples. **e,f,g,h**, n = 3 biologically independent samples. The horizontal lines or centres of the error bars represent the mean values. The error bars represent the s.d. Data were analysed by two-tailed, unpaired t-tests (**b,c**) or two-way ANOVA with Bonferroni's multiple comparisons tests (**e,f,h**).

Methods

Cells. Vero (African green monkey kidney cells), 293T (human embryonic kidney cells transformed by adenovirus and expressing the SV40 T antigen) and Neuro-2a cells (mouse brain neuroblastoma cells) were obtained from ATCC and maintained as described previously³⁰. Construction of 293T138, 293Tcontrol, N2A138, N2AAnt138 and N2AFoxC1 knockout cell lines is described below.

Trigeminal ganglion neurons were isolated and cultured as described previously with slight modifications⁵⁷. Briefly, 6-week-old CD-1 (Institute for Cancer Research) male mice (Charles River Laboratories) were anaesthetized with isoflurane (RWD) for 1 min and transcardially perfused with approximately 10 ml of PBS. Trigeminal ganglia were dissected and digested in collagenase/dispase solution (catalogue nos. C9891 and D4693; Sigma-Aldrich) at 37 °C for 1 h. Neurons were purified by gradient separation in an OptiPrep gradient (catalogue no. D1556; Sigma-Aldrich) followed by two washes with Neurobasal-A medium (catalogue no. 1088022; Thermo Fisher Scientific) + 2% N21-MAX (AR008; R&D Systems). Purified neurons were counted and plated on 10-mm coverslips pretreated with poly-D-lysine (catalogue no. E607014-0002; Sangon Biotech) and laminin (catalogue no. 23017-015; Thermo Fisher Scientific) with 5,000 neurons each. After neurons adhered, the coverslips were transferred to a 24-well plate and cultured in Neurobasal-A medium + 2% N21 + 50 ng ml⁻¹ of neuritin (catalogue no. 1297-NE-025; R&D Systems) + 50 ng ml⁻¹ of neuronal growth factor (catalogue no. 256-GF-100; R&D Systems) + 50 ng ml⁻¹ of glial-derived neurotrophic factor (catalogue no. 212-GD-010; R&D Systems) + 1 µg ml⁻¹ of mitomycin C (catalogue no. HY-13316; MedChemExpress) for 3–4 d.

Human inducible neurogenin3 iSCCs (iNGN3 iSCCs)⁵⁸ were seeded in a Matrigel-coated 6-well plate (1 × 10⁶ cells) and induced with StemFlex medium +



supplement (catalogue no. A3349401; Thermo Fisher Scientific) and 1 µg ml⁻¹ of doxycycline for 4 d. Then, medium was replaced with Neurobasal Plus medium (catalogue no. A3582901; Thermo Fisher Scientific) and DMEM/F-12 (1:1, catalogue no. 11320033, Thermo Fisher Scientific) + B-27 Plus (catalogue no. A3582801; Thermo Fisher Scientific) + N-2 Supplement (catalogue no. 17502001; Thermo Fisher Scientific) + 1× GlutaMAX (catalogue no. 35050079; Thermo Fisher Scientific) + 1× MEM non-essential amino acids solution (catalogue no. 11140050; Thermo Fisher Scientific) and incubated for 5 d with daily medium change, replaced in Neurobasal Plus/DMEM/F-12 + B-27 Plus medium containing 4G (BDNF; 10 ng ml⁻¹; catalogue no. 450-02, PeproTech), GDNF (10 ng ml⁻¹; catalogue no. 450-10, PeproTech), β-NGF (10 ng ml⁻¹; catalogue no. 450-01, PeproTech), NT-3 (10 ng ml⁻¹; catalogue no. 450-03, PeproTech) and ascorbic acid (0.1 mM). To eliminate undifferentiated dividing cells, 5-fluoro-2'-deoxyuridine (20 µM) was added to the medium and maintained for 7–10 d.

Viruses. HSV-1 KOS strain WT and *ICP0*-null mutant virus 7134 were propagated and assayed as described previously³⁹. WT-BAC²⁸, M138 (ref. ²⁶) and WTLyt138 (ref. ³⁰) viruses were generated previously using BAC technology based on the HSV-1 KOS strain. WThomiR138 virus was constructed in the same way as WTLyt138 (named WThmiR138 in this Article) except that in the synthesized gBlocks Gene Fragment³⁰, the miR-138 seed CDS GCTGGTG was replaced with CGACCAC. WThmiR138R virus was generated on the basis of WThomiR138 BAC DNA after the two-step red-mediated recombination protocol³⁹ using the Restore138fw and Restore138rv primers (Supplementary Table 3). The M138miR138, M138nomiR138 and M138miR138R viruses were generated in the same way as WThmiR138, WThomiR138 and WThmiR138R, respectively, starting with M138 BAC DNA. To construct the HSV1FOXC1 and HSV1FOXC1delAD viruses, a DNA cassette coding the kanamycin-resistance (Kan-r) gene plus the I-SceI site was PCR-amplified with the primers Kan3-1F and Kan3-1R and inserted into the NheI site of pcDNAFOXC1human or pcDNAFOXC1delADboth plasmid. The FOXC1-BACF and FOXC1-BACR primers, flanked by approximately 40 base pairs (bp) of the region between US9 and US10 was used to amplify the FOXC1-Kan-r and FOXC1-ADdd-Kan-r cassettes, each including cytomegalovirus promoter and Poly(A) signal sequences. These cassettes were used according to the two-step red-mediated recombination protocol³⁹ to generate BAC genomic DNA, which was transfected into Vero cells to generate viruses. HSV1GFP was constructed in the same way starting from the pcDNAGFP plasmid that we constructed by inserting the EGFP gene between the XhoI and HindIII sites of pcDNA. Virus propagation, titration by plaque assays and infections, which included back titrations of inocula, were performed as described previously³⁰.

Plasmids. pICP0-WT²⁶, pICP0-M13826 and pUL39 (ref. ⁶⁰) were described previously. To construct pFOXC1human and pFOXC1mouse, total human and mouse RNA was extracted from 293T and Neuro-2a cells, respectively using the Easestep Super Total RNA Extraction Kit (Promega Corporation) and reverse-transcribed using the RevertAid First Strand cDNA Synthesis Kit (Thermo Fisher Scientific). FLAG-HA-pcDNA3.1- was obtained from Addgene and designated pcDNA in this study. The Foxfw and FoxHrv primers were used to amplify the human *Foxc1* CDS; the Foxfw and FoxMrv primers were used to amplify the mouse *Foxc1* CDS. Each amplified CDS was inserted between the EcoRI and BamHI sites of pcDNA. The OctHfwa and OctHrvd primers were used to amplify the human *Oct-1* CDS; the OctMfw and OctMrv primers were used to amplify the mouse *Oct-1* CDS. Each amplified CDS was inserted between the XbaI and HindIII sites of pcDNA. Oct-1M1 mutations were introduced into human *Oct-1* site1 using the overlapping PCR method⁴¹. Briefly, using the *Oct-1* CDS fragment as a template, fragment ab was obtained using the Oct-1Hfwa and OctHrvb primers; fragment cd was obtained using the OctHfwd and OctHrvd primers. The overlapping ab and cd fragments were mixed in a 1:1 molar ratio to serve as templates and OctHfwa and OctHrvd served as primers to amplify the *Oct-1* CDS fragment with M1 mutations, which was inserted between the EcoRI and HindIII sites of pOct-1human. To introduce mutations into the human *Oct-1* site2, the Octfwm2 and OctHrvd primers were used to amplify a fragment containing the M2 mutations, which was inserted between the EcoRI and HindIII sites of pOct-1human. pFOXC1delAD-N, pFOXC1delAD-C, pFOXC1delADboth and pFXC1delDBD were constructed by inserting the corresponding PCR products between the EcoRI and BamHI sites of pcDNA. Using the human *Foxc1* CDS as a template, the 1AD-del-F-a1 and Rv-FOXC1-BamHId primers were used to amplify the PCR product for pFOXC1delAD-N; the Fw-FOXC1-EcoRIa and 2AD-del-R-d primers were used for FOXC1delAD-C. The 1AD-del-F-a1 and 2AD-del-R-d primers were used for pFOXC1delADboth. pFOXC1delDBD and FOXC1delID were constructed based on pFOXC1 using the overlapping PCR method. For pFoxc1delDBD, fragment ab was obtained using the Foxfw and FoxKhB primers and fragment cd using the FoxKhC and FoxHrv primers. For pFoxc1delID, fragment ab was obtained using the Fw-FOXC1-EcoRIa and ID-del-r-b primers; fragment cd was obtained using the ID-del-c-f and Rv-FOXC1-BamHId primers. The plasmids for producing lentiviruses LVmiR138 and LVmiRM138b were constructed by inserting the mouse pre-miR-138-1 (with the WT sequence for LVmiR138 and with CGACCAC replacing GCTGGTG of the miR-138 seed region for LVmiRM138b) and flanking sequences (the 146 nucleotide (nt) sequences starting from CCATACTTCA

and ending with ATCCAGACAC were synthesized by Sangong Biotech) into pLVTHMmCherry²² between the MluI and ClaI sites. The GL3 empty vector and luciferase plasmid with the *ICP0* gene promoter of the KOS strain were kind gifts of C. Jones⁶². The luciferase plasmids with the ICP4 and ICP22 promoters of the RE strain were kind gifts of S.-H. Chen⁶³. To construct luciferase plasmids with *Foxc1* 3'-UTR, total human and mouse RNA extracted from 293T and Neuro-2a cells were reverse-transcribed (as described above). The *Foxc1* 3'-UTR fragments were amplified using the lucFwa and lucRvd primers and inserted between the XhoI and NotI sites of psiCheck-2 (Promega Corporation). Then, M1 mutations were introduced into site1 using the overlapping PCR method (see above), with fragment ab obtained using the lucFwa and lucRvb1 primers and fragment cd obtained using the lucFwc1 and lucRvd primers. The M2 mutations were introduced in the same way but using the lucRvb2 and lucFwc2 primers instead of the lucRvb1 and lucFwc1 primers. The sequences of all primers are listed in Supplementary Table 3.

Transfection. Lipofectamine 3000 (Invitrogen) was used according to the manufacturer's protocol. Transfection was performed in 24-well plates with 1 µl of Lipofectamine 3000 reagent per well unless indicated otherwise. Synthetic miRNA mimics were purchased from QIAGEN (miScript miRNA mimic). LNAs were obtained from QIAGEN (miRCURY LNA miRNA power inhibitors for miR-138-5p and negative control B). siRNAs for mouse *Oct-1*, *Foxc1*, *Bcl1* and *Control1* were obtained from QIAGEN. The siRNAs for mouse *Rara* and *Control2* were from Dharmacon. Those for all other mouse genes were custom-designed and synthesized by RiboBio. The sequences of control siRNAs and siRNAs against mouse genes are listed in Supplementary Table 2.

Lentivirus production and transduction of iPSC-derived neurons. 293T cells were plated in a 6-well plate (5×10^5 per well) 1 d before transfection. Cells were transfected with psPAX2:pVSV-G:pLVmiR138 or LVmiRM138b (4:1:5, total 2 or 4 µg) using polyethyleneimine (PEI, catalogue no. 23966; Polysciences). For PEI transfection, 2 or 4 µg of DNA in 200 µl of Opti-MEM (catalogue no. 31985; Gibco) and 6 or 12 µg of PEI in 200 µl of Opti-MEM I were mixed and incubated at room temperature for 20 min. The mixtures were added directly to 293T cells containing 1.5 ml of DMEM (supplemented with 10% vol/vol FBS and 2 mM of glutamine). Cells were incubated at 37 °C for 8–16 h, replaced with 3 ml of fresh DMEM supplemented with 30% vol/vol FBS and 2 mM of glutamine and incubated at 37 °C. Media were collected every 12–24 h for 48–60 h, replaced with fresh DMEM containing 30% FBS and saved on ice. Collected medium was filtered using a 0.45-µm syringe filter (Pall Corporation). Filtered lentivirus containing medium was used directly or concentrated. To concentrate lentivirus, polyethylene glycol 8000 was added to the filtered media (final 10%), incubated on ice for 1 d and centrifuged; supernatant was removed without disrupting the pellet. The pellet was resuspended in cold PBS or DMEM medium (1/10–1/100 of original volume). To transduce cells with lentivirus, lentivirus was added to neurons and spun at 931 g for 0.5–1 h at 25 °C and incubated at 37 °C. The next day, medium was replaced with fresh medium and incubated for 10–14 d at 37 °C.

Western blots. Western blotting was performed as described previously²⁸. The following primary antibodies and dilutions were used: anti-ICP0 antibody (1:5,000, catalogue no. ab6513; Abcam); anti-ICP27 antibody (1:5,000, catalogue no. ab6514; Abcam); anti-ICP27 antibody (1:5,000, catalogue no. 1113; Virusys); anti-thymidine kinase antibody (1:500, catalogue no. sc-28037; Santa Cruz Biotechnology); anti-gC antibody (1:1,000, catalogue no. 10-H25A; Fitzgerald); anti-β-actin antibody (1:10,000, catalogue no. A5441; Sigma-Aldrich); anti-Oct-1 antibody (1:5,000, catalogue no. ab278869; Abcam); anti-FOXC1 antibody (1:500, catalogue no. ab227977; Abcam); anti-β-tubulin antibody (1:5,000, catalogue no. KM9003; Tianjin Sungene Biotech). HRP-conjugated goat anti-mouse, goat anti-rabbit and rabbit anti-goat antibodies (catalogue nos. 1030-05, 4030-05 and 6163-05; SouthernBiotech) were used as secondary antibodies with a dilution of 1:2,000. Uncropped and unprocessed scans of the blots are provided as Source Data files.

RNA-seq. To analyse the effects of miR-138, Neuro-2a and 293T cells were transfected with 40 nM of miR-138 or scrambled mimic RNA with three biological replicates and collected at 24 h post-transfection. Cells were collected and total RNA was purified using an RNeasy Plus Mini Kit (QIAGEN). mRNA was isolated using a Takara mRNA Isolation Kit. Libraries were prepared using a PrepX RNA-seq Library Preparation Kit in an Apollo 324 system (IntegenX). Library quality was confirmed with an Agilent 2200 TapeStation D1000 HS ScreenTape. Sequencing was performed using a NextSeq 500 sequencer (Illumina) by paired-end sequencing of 150 cycles. To analyse the effects of FOXC1, Neuro-2a cells were transfected with 100 ng of pcDNA or pFOXC1human per well (in 4-well plates) for 40 h and infected with KOS (MOI = 1) for 5 h before being collected. RNA purification was the same as above. Library construction and subsequent sequencing were performed by BGI using the BGISEQ500 platform. Reads were trimmed to remove adaptors, low-quality reads and reads less than 30 bases long using Trimmomatic v.0.33 (<http://www.usadellab.org/cms/index.php?page=trimmomatic>). The trimmed reads were aligned to the human (hg19 assembly) or mouse (mm10 assembly) genome using TopHat2 v.2.1.0.

(<https://ccb.jhu.edu/software/tophat/index.shtml>). For alignment to the HSV-1 genome, the KOS sequence was used (GenBank accession no. JQ673480.1), with the terminal repeats (TR_L and TR_S) manually removed. The human and mouse genome files and the corresponding transcript annotation files (in the GTF format) were downloaded from the Harvard Medical School Research Computing server (<https://rc.hms.harvard.edu>). The transcript annotation files (in the GFF format) for the HSV-1 transcripts were created manually according to the format required for a GFF file. The counts of reads aligned to each transcript were determined by HTSeq-count v.0.9.1 (<https://htseq.readthedocs.io>). Viral read counts were normalized by total read counts before being used for the calculation of ratios. Statistical analysis of differentially expressed host transcripts was performed using DESeq2 v.1.30.0 (<https://bioconductor.org/packages/release/bioc/html/DESeq2.html>).

Luciferase assays. Luciferase activities were measured using the Dual Luciferase Reporter Gene Assay Kit (catalogue no. 11402ES60; Yeasen Biotech) and a Cyvation 3 Cell Imaging Multimode Reader (BioTek) according to the manufacturer's instructions.

ChIP. Neuro-2a cells (4×10^6) in a 100-mm plate were transfected with 60 nM of scrambled control, miR-138 or miR-M138b mimics for 24 h using 45 μ l of Lipofectamine 3000 and infected with M138 virus at an MOI of 5. At 6 h post-infection, cells were processed for the ChIP experiments as described previously¹¹. Briefly, cell monolayers were fixed in 1% formaldehyde for 15 min at 37 °C, quenched with 0.125 M of glycine, then lysed for 10 min on ice in 1% SDS lysis buffer (1% SDS, 10 mM of EDTA, 50 mM of Tris, pH 8.1) and sonicated in 15 ml polystyrene tubes at 4 °C in a Diagenode Biorupter for about 6 cycles of 5 min each on the high setting (30 s ON, 30 s OFF) until DNA fragments of approximately 500 bp were obtained. To measure the input genome concentration, 10 μ l (1%) was retained. Each immunoprecipitation reaction was carried out overnight at 4 °C using 15 μ g of chromatin and 2.5 μ g each of the following antibodies: anti-histone H3 (catalogue no. ab1791; Abcam); anti-histone H3K9me3 (catalogue no. ab8898; Abcam); anti-histone H3K27me3 (catalogue no. 39156; Active Motif); or normal rabbit IgG (catalogue no. 12-370; Merck Millipore) in 1 ml of ChIP dilution buffer (150 mM of NaCl, 10 mM of Na_2HPO_4 , 2 mM of EDTA, 1.1% Triton, 0.1% SDS). Immune complexes were captured by rotating with 20 μ l of Magna ChIP Protein A Magnetic Beads (Merck Millipore) for 3 h at 4 °C, after which beads were washed 3 times with a cold low-salt buffer (150 mM of NaCl, 20 mM of Tris-HCl, pH 8.1, 2 mM of EDTA, 1% Triton X-100, 0.1% SDS, 1 mM of phenylmethylsulfonyl fluoride (PMSF)) and 3 times with cold LiCl wash buffer (50 mM of HEPES, pH 7.5, 250 mM of LiCl, 1 mM of EDTA, 1% NP-40, 0.7% sodium deoxycholate, 1 mM of PMSF), followed by 1 wash with cold Tris-EDTA buffer (10 mM of Tris-HCl, pH 8, 1 mM of EDTA). The cross-linked DNA-protein complexes were eluted by incubation with 100 μ l of elution buffer (1% SDS, 0.1 M of $NaHCO_3$) at 65 °C for 10 min. Protein-DNA crosslinks were reversed from input and immunoprecipitates by incubating in 0.2 M of NaCl (final concentration) at 95 °C for 30 min, followed by treatment with 1 μ l of RNase (1 mg ml⁻¹; Ambion) for 1 h at 37 °C and then 2 μ l of proteinase K (Roche) at 45 °C for 2 h. The DNA was then purified using the QIAquick PCR Purification Kit (QIAGEN) and the relative amounts of specific sequences were measured by qPCR¹¹.

qPCR and RT-qPCR. To quantify miR-138 levels in cells, total RNA was purified using an RNeasy Plus Mini Kit following the protocol for retaining small RNAs provided by the manufacturer. Reverse transcription using stem-loop primers and subsequent PCR were carried out using the TaqMan MicroRNA Assay Kit, TaqMan MicroRNA RT Kit and TaqMan Universal PCR master Mix II no UNG (all from Applied Biosystems). miRNA levels were quantified by using standard curves generated from serial dilutions of synthetic miRNAs. To quantify the viral genome and transcripts in mouse trigeminal ganglia, DNA and RNA were isolated using a DNA/RNA Isolation Kit (TIANGEN) or Easy RNA Extraction Kit (catalogue no. DR0401050; Easy-Do Biotech); reverse transcription and PCR were conducted using a HiScript II Q Select RT SuperMix and ChamQ Universal SYBR qPCR Kit (catalogue nos. R233-01 and Q711-02/03; Vazyme Biotech). Previously described primers and DNA and RNA standards²⁶ were used. Viral genome levels were normalized to mouse *Adipsin* gene levels. Viral transcript levels were normalized to *GAPDH* transcript levels and then to viral genome levels. To analyse the candidate host targets of miR-138, standard curves were generated using serially diluted RNA from control siRNA-transfected cells. The primer sequences for the host transcripts are listed in Supplementary Table 2.

Northern blot analysis. 293T cells (2×10^7) in a 100-mm plate were infected with M138Lyt138 or M138Lyt138 knockout virus at an MOI of 5. At 8 h post-infection, the RNA of <200 nt was purified from the cells using an miRNeasy Mini kit (QIAGEN). RNA was resolved on Novex 15% Tris-borate-EDTA-urea polyacrylamide gels (Thermo Fisher Scientific) alongside serially diluted synthetic miR-138 or miR-M138b (Integrated DNA Technologies). Northern blot hybridization used a previously described non-radioactive method²⁴ and synthetic miR-138 and miR-M138b LNA probes with digoxigenin labelled at 3'-ends (synthesized by QIAGEN). The miR-138 probe has this

sequence: CGGCCTG + A + TT + C + A + CA + ACACCAAGCT, where +N indicates an LNA-modified nucleotide. The miR-M138b probe has this sequence: GCCTGAT + TCAC + AA + GTG + GT + CGT. Hybridization and washing were conducted at 60 °C for both miRNAs.

Mouse procedures. Male CD-1 (Institute for Cancer Research) mice were purchased from the Shanghai Laboratory Animals Center. Mouse housing and experimental procedures were approved by the Animal Research Committee of Zhejiang University in accordance with national guidelines. Mice were housed at ambient temperature (approximately 23 °C) with low humidity in an air-conditioned room with 12 h light-dark cycles. Six-week-old mice were anaesthetized by intraperitoneal injection of 0.4 ml of a mixture containing 4 mg ml⁻¹ pentobarbital sodium (Solarbio) and 500 μ g ml⁻¹ xylazine hydrochloride (catalogue no. X1251; Sigma-Aldrich) in sterile saline. Then, 2×10^5 or 4×10^4 plaque-forming units (p.f.u.) of virus in 3 μ l was dropped onto each scarified cornea. To collect the eye swabs, mice were anaesthetized with 3% isoflurane (RWD Life Science) in oxygen with a flow rate of 0.5 ml min⁻¹ using a V1 Table Top anaesthesia machine (Colonial Medical Supply). Both eyes of each mouse were swabbed with cotton-tipped applicators, which were suspended in 1 ml of cell culture medium. For trigeminal ganglion acquisition, mice were killed by cervical dislocation and the trigeminal ganglia were removed and placed on dry ice before storing at -80 °C. Trigeminal ganglia were homogenized in cell culture medium for the virus titres. To analyse the nucleic acids, trigeminal ganglia were homogenized in lysis buffer (see above).

Construction of lentivirus-transduced cell lines. The pre-miR-138-1-expressing and flanking sequences were amplified from Neuro-2a cells using the Trip138fw and Trip138rv primers (Supplementary Table 3) and inserted between the XbaI and EcoRI restriction sites of pTRIPZ⁶⁵ (a generous gift from B. Cullen). An aliquot (4 μ g) of the resulting plasmid or empty vector was transfected together with 7.1 μ g of psPAX2 plasmid (Addgene) and 3.9 μ g of the pMD2.G plasmid (Addgene) into 293T cells in a 100-mm plate using Lipofectamine 3000 according to the manufacturer's instructions (Thermo Fisher Scientific). Lentiviruses were collected from the supernatants at 3 d post-transfection and added to 50% confluent 293T or Neuro-2a cells with 8 μ g ml⁻¹ of hexadimethrine bromide (Sigma-Aldrich). Two days later, the supernatant was removed and replaced with fresh medium containing 1 μ g ml⁻¹ puromycin. Surviving cells were expanded in the presence of 1 μ g ml⁻¹ puromycin. The N2Aanti138 cell line was constructed in the same way except that a fragment antisense to miR-138 was inserted into the pTRIPZ vector. The fragment was made by annealing synthetic oligonucleotide DNA TripAnti138fw and TripAnti138rv (Supplementary Table 3). Annealing was achieved by mixing 4 μ M of each oligonucleotide in annealing buffer (30 mM of HEPES-KOH, pH 7.4, 100 mM of potassium acetate, 2 mM of magnesium acetate), incubating the mixture at 98 °C for 10 min on a heat block and slowly cooling down to room temperature.

PAR-CLIP. PAR-CLIP was carried out as described previously⁶⁶ with some modifications. 293T138, 293Tcontrol, N2A138 and N2Aanti138 cells were expanded in the presence of 1 μ g ml⁻¹ doxycycline for 3 d. Twenty 100-mm plates of cells of approximately 90% confluence were used for each condition. The ribonucleotide 4-thiouridine (Sigma-Aldrich) was added (100 μ M). Crosslinking was performed at 18 h after adding 4-thiouridine to uninfected cells. For infection, 18 h after adding 4-thiouridine, 293T138 and 293Tcontrol cells were infected with WT virus for 4 or 8 h (MOI = 1) before crosslinking. For crosslinking, the medium was removed and cells were irradiated on ice with 0.15 J cm⁻² of 365 nm ultraviolet light. Then, 4 ml of PBS was added to each plate. The cells for each condition were scraped into the buffer, pooled and centrifuged at 400 g at 4 °C for 5 min. The supernatant was discarded and the cell pellet was snap-frozen in liquid nitrogen and stored at -80 °C.

The frozen pellet was resuspended in 9 ml of NP-40 lysis buffer (50 mM of HEPES-KOH, pH 7.5, 150 mM of KCl, 2 mM of EDTA-NaOH, 1 mM of NaF, 0.5% NP-40, 0.5 mM of dithiothreitol (DTT), complete EDTA-free protease inhibitor cocktail (Roche)), incubated on ice for 10 min and centrifuged at 13,000 r.p.m. at 4 °C for 20 min. The pellet was discarded. RNase T1 (Thermo Fisher Scientific) was added to the supernatant to a final concentration of 100 μ M. The tube was incubated for 15 min at 22 °C and then placed on ice for >5 min. At the same time, antibody-conjugated beads were prepared as follows. For each sample, 200 μ l of Protein G Dynabeads (Thermo Fisher Scientific) were transferred to a 1.5 ml tube, washed twice with 1 ml of PBS on a magnetic particle collector on ice and resuspended in 200 μ l of PBS. Rabbit anti-mouse IgG Fcγ fragment (catalogue no. 315-005-008; Jackson ImmunoResearch) (60 μ g) was added as a bridging antibody. The tube was rotated at room temperature for 1 h. Beads were washed twice with 1 ml of PBS and resuspended in 100 μ l of PBS plus 50 μ g of 2A8 Anti-pan AGO antibody (clone 2A8, catalogue no. MABE56; Merck Millipore). These beads were then added to the cell lysates and incubated on a rotating wheel overnight at 4 °C.

Beads were collected on a magnetic particle collector and the supernatant was discarded. Beads were resuspended in 1 ml of immunoprecipitation wash buffer (50 mM of HEPES-KOH, pH 7.5, 300 mM of KCl, 0.05% NP-40, 0.5 mM of DTT, complete EDTA-free protease inhibitor cocktail) and transferred to a 1.5 ml tube.

Beads were washed 4 times (10 min each) with 1 ml of immunoprecipitation wash buffer on a rotating wheel and resuspended in 200 µl of immunoprecipitation wash buffer. RNaseT1 was added to a final concentration of 40 µg µl⁻¹. Beads were incubated at 22 °C for 15 min, then on ice for 5 min before being washed 4 times (10 min each) with 1 ml of high-salt wash buffer (same as the immunoprecipitation wash buffer except that the KCl concentration was 500 mM) on a rotating wheel and resuspended in 200 µl of dephosphorylation buffer (50 mM of Tris-HCl, pH 7.9, 100 mM of NaCl, 10 mM of MgCl₂, 1 mM of DTT). Then, 100 µg of calf intestinal alkaline phosphatase (New England Biolabs) was added and the tube was incubated at 37 °C for 30 min. Beads were washed 3 times with 1 ml of phosphatase wash buffer (50 mM of Tris-HCl, pH 7.5, 20 mM of EGTA-NaOH, 0.5% NP-40), then twice with 1 ml of polynucleotide kinase (PNK) buffer without DTT (50 mM of Tris-HCl, pH 7.5, 50 mM of NaCl, 10 mM of MgCl₂) and resuspended in 200 µl of PNK buffer (50 mM of Tris-HCl, pH 7.5, 50 mM of NaCl, 10 mM of MgCl₂, 5 mM of DTT). [γ -³²P] ATP (PerkinElmer) (20 µCi) and T4 PNK (New England Biolabs) (200 µg) was added and the tube was incubated at 37 °C for 20 min. Then, 10 µl of 10 mM of ATP was added and the tube was incubated at 37 °C for another 10 min. Beads were washed 6 times with 900 µl of PNK buffer without DTT for 10 min each time. Some supernatant after the first wash was saved to label the membrane described below. Beads were resuspended in 70 µl of SDS-polyacrylamide gel electrophoresis (PAGE) loading buffer (10% glycerol v/v, 50 mM of Tris-HCl, pH 6.8, 2 mM of EDTA, 2% SDS w/v, 100 mM of DTT, 0.1% bromophenol blue) and incubated at 95 °C for 5 min to elute the protein-RNA complex and vortexed. The supernatant was separated from the beads on a magnetic particle collector, transferred to a 1.5 ml tube and stored at -20 °C.

The protein-RNA complex was separated on a Novex Bis-Tris 4–12% precast protein gel (Thermo Fisher Scientific) in MOPS-SDS running buffer (Thermo Fisher Scientific) at 200 V for 40 min. The cross-linked complex on the gel was transferred using a wet transfer apparatus onto a 0.45-µm nitrocellulose membrane (Thermo Fisher Scientific) in NuPAGE transfer buffer (Thermo Fisher Scientific) at 100 V for 1 h. The membrane was labelled at 3 corners by spotting 0.5 µl of the radioactive wash collected above, wrapped in plastic film and exposed to a phosphor screen and visualized by a phosphorimager. The image was printed at its original size. The bands corresponding to the AGO-RNA complex of 100–140 kDa (Fig. 4b) were cut out using a razor blade, further cut into 6 pieces and transferred to a 1.5-ml low adhesion tube (USA Scientific). Proteinase K (Roche) (400 µl of 5 mg ml⁻¹) in proteinase K buffer (50 mM of Tris-HCl, pH 7.5, 6.25 mM of EDTA-NaOH, pH 8.0, 75 mM of NaCl, 1% SDS) was added to the nitrocellulose pieces and the tube was incubated at 55 °C with shaking at 1,000 r.p.m. for 1.5 h. RNA was extracted by adding 800 µl of acid phenol/chloroform (pH 4.5; Ambion) and shaking vigorously. After centrifugation at 13,000 r.p.m. at 4 °C for 10 min, the upper aqueous layer was transferred to another tube. This extraction was repeated once. The RNA was then similarly extracted twice with 400 µl of chloroform. After the last extraction, the upper phase was transferred to a new 1.5-ml low adhesion tube. One tenth volume of 3 M NaAc (pH 5.2), 2.5 µg of glycogen (Thermo Fisher Scientific) and 3 volumes of 100% ethanol were added and mixed. This mixture was stored at -20 °C overnight to precipitate RNA. The sample was centrifuged at 14,000 r.p.m. at 4 °C for 30 min and the pellet was washed twice with 1 ml of ice-cold 75% ethanol. The final pellet was air-dried and dissolved in 15 µl of water.

The RNA sample was used for library preparation with a TruSeq Small RNA Library Preparation Kit (Illumina) according to the manufacturer's protocol. The optimal cycle number for PCR was determined to be 18 (Extended Data Fig. 5b) based on the criterion that it should be within the exponential amplification phase of PCR⁶⁶. After the final PCR and PAGE, bands of 135–180 bp (corresponding to 15–60 base RNA) were cut out. DNA was eluted and purified from the bands according to the Illumina protocol and submitted for Illumina sequencing.

Sequencing was performed using a NextSeq 500 sequencer by single-end sequencing of 50 cycles. Reads were trimmed to discard adaptors, low-quality reads and reads less than 21 bases long using fastx_clipper v.0.1.13 (http://hannonlab.cshl.edu/fastx_toolkit/). Reads containing the CACCAGC sequence (the binding site of the miR-138 seed region) were retained using the 'grep' command. These reads were aligned to the human (hg19 version) or mouse (mm10 version) genome or HSV-1 KOS strain genome using TopHat2 v.2.1.0. Annotation files of 5'-UTR, CDS and 3'-UTR for human and mouse transcripts were downloaded from the University of California, Santa Cruz genome browser in BED format (genome.ucsc.edu). The BED files were converted to GFF files by bedtools v.2.27.1 (<https://bedtools.readthedocs.io>). Read counts for 5'-UTR, CDS and 3'-UTR of each transcript were determined by HTSeq-count v.0.9.1.

Immunofluorescence assays. To analyse Neuro-2a cells and primary trigeminal ganglion neurons, cells were fixed in 4% paraformaldehyde (PFA) for 10 min and washed with PBS for 5 min. Cells were permeabilized in 0.1% Triton X-100 in PBS for 10 min and washed with PBS 3 times for 5 min each. Cells were blocked with 1% BSA in PBS for 1 h at room temperature and then incubated with primary antibody at 4 °C overnight and washed 3 times for 10 min each. Cells were incubated with secondary antibody for 1 h and then with 2 µg ml⁻¹ 4,6-diamidino-2-phenylindole (DAPI) for 10 min before being washed 4 times with PBS for 10 min each. The coverslips were mounted onto microscope slides with the anti-fading reagent Fluoromount-G (catalogue no. 0100-01; SouthernBiotech).

Images were acquired on a Nikon Eclipse Ti-S inverted microscope with a $\times 100$ magnification using the Oplenix v.X64 software. Images were analysed using ImageJ v.1.52n (National Institutes of Health).

To analyse mouse trigeminal ganglia, uninfected six-week-old male CD-1 mice or mice infected for 3 d were anaesthetized with isoflurane and cardiac perfusion was immediately performed with 30 ml of PBS followed by 30 ml of 4% PFA for fixation. After mice were fixed on ice for 1 h, trigeminal ganglia were dissected and fixed in 4% PFA overnight followed by dehydration in 30% sucrose for at least 24 h. Trigeminal ganglia were embedded and 10-µm sections were prepared on a CryoStar NX50 Cryostat (Thermo Fisher Scientific) and plated onto glass microscope slides. Trigeminal ganglion sections were first immersed in 0.2% Triton X-100 in PBS for 10 min. After 3 washes in PBS for 10 min each, they were blocked in 1% BSA in PBS for 1 h at room temperature and incubated with primary antibody at 4 °C overnight. After 3 washes in PBS for 10 min each, they were incubated with secondary antibody for 1 h. DAPI staining, washing, mounting and image acquisition were the same as above except that a $\times 40$ magnification was used. The following antibodies and dilutions were used: rabbit anti-FOXC1, 1:100; rabbit anti-Oct-1, 1:400; mouse anti-Tuj1 antibody (1:2,000, catalogue no. ab78078; Abcam); mouse anti-FLAG antibody (1:1,000, catalogue no. F1804; Sigma-Aldrich); goat anti-mouse IgG H&L Alexa Fluor 488 (1:500, ab150117; Abcam); and goat anti-rabbit IgG Alexa Fluor 555 (1:1,000 catalogue no. 4413s; Cell Signaling Technology); goat anti-mouse IgG Alexa Fluor 568 (1:1,000, catalogue no. A11004; Thermo Fisher Scientific); donkey anti-rabbit IgG H&L Alexa Fluor 405 (1:1,000, catalogue no. ab175651; Abcam).

AAV-transduction and HSV-1 infection of primary trigeminal ganglion

neurons. The CDS of human FOXC1 or its FOXC1delAD mutant was inserted into the AAV-CAG-GFP (catalogue no. 37825; Addgene) plasmid between the AgeI and HindIII restriction enzymes digestion sites. After confirmation of their expression and effects on HSV-1 replication in Neuro-2a cells (data not shown), both plasmids were sent to Vigenebio for AAV packaging. Three days after isolation and culture, trigeminal ganglion neurons from each well were transduced with AAV containing 7×10^9 genome copies. Five days later, neurons were infected with HSV1GFP at an MOI of 2 or 10, as indicated. Then, 40 µl of supernatant were withdrawn from each well at the time points indicated for virus titration. At 72 h post-infection, neurons were fixed and analysed by immunofluorescence assays.

Attachment and nuclear entry assays. Neuro-2a cells in 6-well plates were transfected with 500 ng per well of pFOXC1delADboth or pFOXC11delID per well using Lipofectamine 3000 for 40 h before infection. For infection, cells were incubated at 4 °C for 30 min before the addition of virus (MOI = 2) on ice. Cells were incubated at 4 °C for 1 h with gentle rocking every 15 min to allow attachment of virus to cells. To analyse attachment, medium containing virus was removed and cells were washed on ice three times with cold PBS before being collected for viral genome analysis by qPCR (see above). To measure the amounts of virus that entered the nucleus, after the 1-h incubation at 4 °C, medium containing virus was removed and replaced with prewarmed fresh medium before cells were incubated at 37 °C for 2 h. Cells (after the 37 °C incubation or, as a control, right after attachment at 4 °C) were washed once with cold PBS and scraped into 1 ml of cold PBS containing 0.5 mg ml⁻¹ of proteinase K (TransGen Biotech) and incubated at 4 °C for 2 h. Then, cells were washed three times with 1 ml of cold PBS each by centrifugation at 3,500 r.p.m. for 3 min followed by replacing the supernatant and resuspension. After the last wash, cells were centrifuged and resuspended and then incubated on ice in 1 ml of an ice-cold hypotonic buffer (10 mM of HEPES, pH 7.9, 1.5 mM of MgCl₂, 10 mM of KCl, 0.5 mM of DTT). Cells were transferred into a 1-ml Dounce homogenizer and subjected to 15 strokes of homogenization using a tight pestle. Cells were transferred to another tube and centrifuged at 5,000 r.p.m. and 4 °C for 5 min. The supernatant was discarded and the pellet containing the nuclear fraction was collected for qPCR analysis of viral genome levels (see above).

Construction of the N2AFOXC1 knockout cell line by CRISPR-Cas9

technology. The N2AFOxc1 knockout cell line was generated using a method described previously⁶⁷; the target sequence, CTGCGCGTATAAGGCCGTAGG, corresponded to nucleotides 188–210 of the mouse *Foxc1* coding region (Fig. 7A). Synthetic oligonucleotides were designed as described by Ran et al.⁶⁷ and cloned into the PX459 vector that expresses Cas9 (Addgene). Neuro-2a cells (1.0 \times 10⁵) in a 24-well plate were transfected with 200 ng of the resulting plasmid. At 24 h, the supernatant was replaced with fresh medium and cells were transfected again. At 24 h after the second transfection, the medium was replaced with fresh medium containing 1 µg ml⁻¹ of puromycin. At 48 h, cells were washed with PBS and trypsinized. One portion of the cells was used for a T7 endonuclease I assay⁶⁷, which showed successful editing at the desired location (data not shown). The other portion was diluted and seeded in 96-well plates with a density of 0.5 cells per well in the presence of 0.5 µg ml⁻¹ of puromycin. Wells with single cells were labelled after 12 h of complete adherence. When cells were confluent, they were trypsinized and transferred to a 24-well plate for expansion. When the cells were confluent again, a portion was used for further expansion in medium with 0.5 µg ml⁻¹ of puromycin. The remaining cells were used for genomic DNA extraction using the Tissue & Cell Genomic DNA Purification Kit (GeneMark),

followed by PCR using the primers GAAGTTGATCCGAACGTTCCCTC and GTCGAGCGTCCAGTAGCTGC and then sequencing using these primers. Of the 20 single-cell colonies, only 1 colony gave clean sequencing data, with a deletion of 19 nt (Extended Data Fig. 9a). The expanded cell line was designated N2AFOXC1 knockout.

Statistical analyses. Analysis of differentially expressed genes in the RNA-seq data was performed using DESeq2 v.1.30.0 (<https://bioconductor.org/packages/release/bioc/html/DESeq2.html>). Other statistical analyses were performed using Prism 7.00 for Windows (GraphPad Software, www.graphpad.com). All measurements were taken from distinct samples. The tests used are indicated in the figure legends.

Reporting Summary. Further information on research design is available in the Nature Research Reporting Summary linked to this article.

Data availability

Raw high-throughput sequencing data for RNA-seq (Figs. 1g and 3 and Extended Data Figs. 2 and 8b) and PAR-CLIP (Fig. 3 and Extended Data Fig. 5) experiments have been deposited with the Gene Expression Omnibus under accession no. GSE127504. The HSV-1 KOS strain genome sequence and annotation were obtained from GenBank with accession no. JQ673480.1. Human (hg19) and mouse (mm10) genome sequences and annotations were downloaded from the Harvard Medical School Research Computing server (<https://rc.hms.harvard.edu>). Source data are provided with this paper.

Received: 25 March 2019; Accepted: 20 November 2020;

Published online: 8 February 2021

References

- Bartel, D. P. Metazoan microRNAs. *Cell* **173**, 20–51 (2018).
- Ebert, M. S. & Sharp, P. A. Roles for microRNAs in conferring robustness to biological processes. *Cell* **149**, 515–524 (2012).
- Guo, Y. E. & Steitz, J. A. Virus meets host microRNA: the destroyer, the booster, the hijacker. *Mol. Cell. Biol.* **34**, 3780–3787 (2014).
- Bruscella, P. et al. Viruses and miRNAs: more friends than foes. *Front. Microbiol.* **8**, 824 (2017).
- Girardi, E., López, P. & Pfeffer, S. On the importance of host microRNAs during viral infection. *Front. Genet.* **9**, 439 (2018).
- Skalsky, R. L. & Cullen, B. R. Viruses, microRNAs, and host interactions. *Annu. Rev. Microbiol.* **64**, 123–141 (2010).
- Roizman, B. et al. in *Fields Virology* 6th edn (eds Knipe, D.M. et al.) 1823–1897 (Lippincott Williams & Wilkins, 2013).
- Wysocka, J. & Herr, W. The herpes simplex virus VP16-induced complex: the makings of a regulatory switch. *Trends Biochem. Sci.* **28**, 294–304 (2003).
- Nogueira, M. L., Wang, V. E. H., Tantin, D., Sharp, P. A. & Kristie, T. M. Herpes simplex virus infections are arrested in Oct-1-deficient cells. *Proc. Natl Acad. Sci. USA* **101**, 1473–1478 (2004).
- Cai, W. & Schaffer, P. A. Herpes simplex virus type 1 ICP0 regulates expression of immediate-early, early, and late genes in productively infected cells. *J. Virol.* **66**, 2904–2915 (1992).
- Lee, J. S., Raja, P. & Knipe, D. M. Herpesviral ICP0 protein promotes two waves of heterochromatin removal on an early viral promoter during lytic infection. *mBio* **7**, e02007-15 (2016).
- Oh, J. & Fraser, N. W. Temporal association of the herpes simplex virus genome with histone proteins during a lytic infection. *J. Virol.* **82**, 3530–3537 (2008).
- Cliffe, A. R. & Knipe, D. M. Herpes simplex virus ICP0 promotes both histone removal and acetylation on viral DNA during lytic infection. *J. Virol.* **82**, 12030–12038 (2008).
- Herrera, F. J. & Triezenberg, S. J. VP16-dependent association of chromatin-modifying coactivators and underrepresentation of histones at immediate-early gene promoters during herpes simplex virus infection. *J. Virol.* **78**, 9689–9696 (2004).
- Kwiatkowski, D. L., Thompson, H. W. & Bloom, D. C. The polycomb group protein Bmi1 binds to the herpes simplex virus 1 latent genome and maintains repressive histone marks during latency. *J. Virol.* **83**, 8173–8181 (2009).
- Cliffe, A. R., Coen, D. M. & Knipe, D. M. Kinetics of facultative heterochromatin and polycomb group protein association with the herpes simplex viral genome during establishment of latent infection. *mBio* **4**, e00590-12 (2013).
- Raja, P. et al. A herpesviral lytic protein regulates the structure of latent viral chromatin. *mBio* **7**, e00633-16 (2016).
- Cliffe, A. R., Garber, D. A. & Knipe, D. M. Transcription of the herpes simplex virus latency-associated transcript promotes the formation of facultative heterochromatin on lytic promoters. *J. Virol.* **83**, 8182–8190 (2009).
- Wang, Q.-Y. et al. Herpesviral latency-associated transcript gene promotes assembly of heterochromatin on viral lytic-gene promoters in latent infection. *Proc. Natl Acad. Sci. USA* **102**, 16055–16059 (2005).
- Umbach, J. L. et al. MicroRNAs expressed by herpes simplex virus 1 during latent infection regulate viral mRNAs. *Nature* **454**, 780–783 (2008).
- Jurak, I. et al. Numerous conserved and divergent microRNAs expressed by herpes simplex viruses 1 and 2. *J. Virol.* **84**, 4659–4672 (2010).
- Kim, J. Y., Mandarino, A., Chao, M. V., Mohr, I. & Wilson, A. C. Transient reversal of episome silencing precedes VP16-dependent transcription during reactivation of latent HSV-1 in neurons. *PLoS Pathog.* **8**, e1002540 (2012).
- Linderman, J. A. et al. Immune escape via a transient gene expression program enables productive replication of a latent pathogen. *Cell Rep.* **18**, 1312–1323 (2017).
- Du, T., Zhou, G. & Roizman, B. HSV-1 gene expression from reactivated ganglia is disordered and concurrent with suppression of latency-associated transcript and miRNAs. *Proc. Natl Acad. Sci. USA* **108**, 18820–18824 (2011).
- Thompson, R. L., Preston, C. M. & Sawtell, N. M. De novo synthesis of VP16 coordinates the exit from HSV latency in vivo. *PLoS Pathog.* **5**, e1000352 (2009).
- Pan, D. et al. A neuron-specific host microRNA targets herpes simplex virus-1 ICP0 expression and promotes latency. *Cell Host Microbe* **15**, 446–456 (2014).
- Bogerd, H. P. et al. Replication of many human viruses is refractory to inhibition by endogenous cellular microRNAs. *J. Virol.* **88**, 8065–8076 (2014).
- Pan, D. & Coen, D. M. Quantification and analysis of thymidine kinase expression from acyclovir-resistant G-string insertion and deletion mutants in herpes simplex virus-infected cells. *J. Virol.* **86**, 4518–4526 (2012).
- Cai, W. Z. & Schaffer, P. A. Herpes simplex virus type 1 ICP0 plays a critical role in the de novo synthesis of infectious virus following transfection of viral DNA. *J. Virol.* **63**, 4579–4589 (1989).
- Pan, D. et al. Herpes simplex virus 1 lytic infection blocks microRNA (miRNA) biogenesis at the stage of nuclear export of pre-miRNAs. *mBio* **10**, e02856-18 (2019).
- Haraguchi, T., Ozaki, Y. & Iba, H. Vectors expressing efficient RNA decoys achieve the long-term suppression of specific microRNA activity in mammalian cells. *Nucleic Acids Res.* **37**, e43 (2009).
- Gilding, L. N. & Somervaille, T. C. P. The diverse consequences of FOXC1 deregulation in cancer. *Cancers (Basel)* **11**, 184 (2019).
- Berry, F. B., Saleem, R. A. & Walter, M. A. FOXC1 transcriptional regulation is mediated by N- and C-terminal activation domains and contains a phosphorylated transcriptional inhibitory domain. *J. Biol. Chem.* **277**, 10292–10297 (2002).
- Wang, W., Zhao, L.-J., Tan, Y.-X., Ren, H. & Qi, Z.-T. MiR-138 induces cell cycle arrest by targeting cyclin D3 in hepatocellular carcinoma. *Carcinogenesis* **33**, 1113–1120 (2012).
- Sossey-Alaoui, K. & Plow, E. F. miR-138-mediated regulation of KINDLIN-2 expression modulates sensitivity to chemotherapeutics. *Mol. Cancer Res.* **14**, 228–238 (2016).
- Huang, H. et al. MIR-138-5P inhibits the progression of prostate cancer by targeting FOXC1. *Mol. Genet. Genomic Med.* **8**, e1193 (2020).
- Yu, C. et al. MicroRNA-138-5p regulates pancreatic cancer cell growth through targeting FOXC1. *Cell. Oncol. (Dordr.)* **38**, 173–181 (2015).
- Bai, X. et al. Inhibition of lung cancer growth and metastasis by DHA and its metabolite, RvD1, through miR-138-5p/FOXC1 pathway. *J. Exp. Clin. Cancer Res.* **38**, 479 (2019).
- Siegel, G. et al. A functional screen implicates microRNA-138-dependent regulation of the depalmitoylation enzyme APT1 in dendritic spine morphogenesis. *Nat. Cell Biol.* **11**, 705–716 (2009).
- Wang, X. et al. MicroRNA-138 promotes tau phosphorylation by targeting retinoic acid receptor alpha. *FEBS Lett.* **589**, 726–729 (2015).
- Yeh, Y.-M., Chuang, C.-M., Chao, K.-C. & Wang, L.-H. MicroRNA-138 suppresses ovarian cancer cell invasion and metastasis by targeting SOX4 and HIF-1α. *Int. J. Cancer* **133**, 867–878 (2013).
- Acharya, M., Huang, L., Fleisch, V. C., Allison, W. T. & Walter, M. A. A complex regulatory network of transcription factors critical for ocular development and disease. *Hum. Mol. Genet.* **20**, 1610–1624 (2011).
- Iwafuchi-Doi, M. et al. The pioneer transcription factor FoxA maintains an accessible nucleosome configuration at enhancers for tissue-specific gene activation. *Mol. Cell* **62**, 79–91 (2016).
- O'Connor, C. M., Vanicek, J. & Murphy, E. A. Host microRNA regulation of human cytomegalovirus immediate early protein translation promotes viral latency. *J. Virol.* **88**, 5524–5532 (2014).
- Trobaugh, D. W. et al. RNA viruses can hijack vertebrate microRNAs to suppress innate immunity. *Nature* **506**, 245–248 (2014).
- Ruelas, D. S. et al. MicroRNA-155 reinforces HIV latency. *J. Biol. Chem.* **290**, 13736–13748 (2015).
- Jopling, C. L., Yi, M., Lancaster, A. M., Lemon, S. M. & Sarnow, P. Modulation of hepatitis C virus RNA abundance by a liver-specific microRNA. *Science* **309**, 1577–1581 (2005).

48. Mulik, S. et al. Role of miR-132 in angiogenesis after ocular infection with herpes simplex virus. *Am. J. Pathol.* **181**, 525–534 (2012).
49. Bhela, S. et al. Critical role of microRNA-155 in herpes simplex encephalitis. *J. Immunol.* **192**, 2734–2743 (2014).
50. Ingle, H. et al. The microRNA miR-485 targets host and influenza virus transcripts to regulate antiviral immunity and restrict viral replication. *Sci. Signal.* **8**, ra126 (2015).
51. Sawtell, N. M. & Thompson, R. L. De novo herpes simplex virus VP16 expression gates a dynamic programmatic transition and sets the latent/lytic balance during acute infection in trigeminal ganglia. *PLoS Pathog.* **12**, e1005877 (2016).
52. Tal-Singer, R. et al. The transcriptional activation domain of VP16 is required for efficient infection and establishment of latency by HSV-1 in the murine peripheral and central nervous systems. *Virology* **259**, 20–33 (1999).
53. Stern, S., Tanaka, M. & Herr, W. The Oct-1 homoeodomain directs formation of a multiprotein-DNA complex with the HSV transactivator VP16. *Nature* **341**, 624–630 (1989).
54. Whitlow, Z. & Kristie, T. M. Recruitment of the transcriptional coactivator HCF-1 to viral immediate-early promoters during initiation of reactivation from latency of herpes simplex virus type 1. *J. Virol.* **83**, 9591–9595 (2009).
55. Kolb, G. & Kristie, T. M. Association of the cellular coactivator HCF-1 with the Golgi apparatus in sensory neurons. *J. Virol.* **82**, 9555–9563 (2008).
56. Elliott, G. & O'Hare, P. Equine herpesvirus 1 gene 12, the functional homologue of herpes simplex virus VP16, transactivates via octamer sequences in the equine herpesvirus IE gene promoter. *Virology* **213**, 258–262 (1995).
57. Katzenell, S., Cabrera, J. R., North, B. J. & Leib, D. A. Isolation, purification, and culture of primary murine sensory neurons. *Methods Mol. Biol.* **1656**, 229–251 (2017).
58. Ng, A. H. M. et al. A comprehensive library of human transcription factors for cell fate engineering. *Nat. Biotechnol.* <https://doi.org/10.1038/s41587-020-0742-6> (2020).
59. Tischer, B. K., von Einem, J., Kaufer, B. & Osterrieder, N. Two-step red-mediated recombination for versatile high-efficiency markerless DNA manipulation in *Escherichia coli*. *Biotechniques* **40**, 191–197 (2006).
60. Sen, J., Liu, X., Roller, R. & Kniipe, D. M. Herpes simplex virus US3 tegument protein inhibits Toll-like receptor 2 signaling at or before TRAF6 ubiquitination. *Virology* **439**, 65–73 (2013).
61. Heckman, K. L. & Pease, L. R. Gene splicing and mutagenesis by PCR-driven overlap extension. *Nat. Protoc.* **2**, 924–932 (2007).
62. Sinani, D., Cordes, E., Workman, A., Thunuguntia, P. & Jones, C. Stress-induced cellular transcription factors expressed in trigeminal ganglionic neurons stimulate the herpes simplex virus 1 ICP0 promoter. *J. Virol.* **87**, 13042–13047 (2013).
63. Chen, S.-H. et al. Suppression of transcription factor early growth response 1 reduces herpes simplex virus lethality in mice. *J. Clin. Invest.* **118**, 3470–3477 (2008).
64. Pan, D., Pesola, J. M., Li, G., McCarron, S. & Coen, D. M. Mutations inactivating herpes simplex virus 1 microRNA miR-H2 do not detectably increase ICP0 gene expression in infected cultured cells or mouse trigeminal ganglia. *J. Virol.* **91**, e02001-16 (2017).
65. Gottwein, E. & Cullen, B. R. A human herpesvirus microRNA inhibits p21 expression and attenuates p21-mediated cell cycle arrest. *J. Virol.* **84**, 5229–5237 (2010).
66. Danan, C., Manickavel, S. & Hafner, M. PAR-CLIP: a method for transcriptome-wide identification of RNA binding protein interaction sites. *Methods Mol. Biol.* **1358**, 153–173 (2016).
67. Ran, F. A. et al. Genome engineering using the CRISPR-Cas9 system. *Nat. Protoc.* **8**, 2281–2308 (2013).

Acknowledgements

We thank B. Cullen, C. Jones and S.-H. Chen for the generous provision of plasmids, K. Holton from Harvard Medical School Research Computing for help with the sequencing data analysis, and the Core Facility of Zhejiang University School of Medicine and the Biopolymers Facility at Harvard Medical School for expertise and instrument availability. This work was supported by the National Key R & D Program of China (no. 2017YFC1200204 to D.P.), National Natural Science Foundation of China (no. 81671993 to D.P.), Natural Science Foundation of Zhejiang Province, China (no. LR18H190001 to D.P.), National Institutes of Health (no. P01 AI098681 to D.M.C. and D.M.K.), a Harvard Medical School Dean's Initiative for Innovation Grant (D.M.K. and D.M.C.), a Natural Sciences and Engineering Research Council of Canada Postgraduate Fellowship and a Peter and Carolyn Lynch Foundation Fellowship (to A.H.M.N.), the National Human Genome Research Institute (no. RM1 HG008525 to G.M.C.) and the Blavatnik Biomedical Accelerator at Harvard University (to G.M.C.).

Author contributions

D.P. conceived the study. B.S., X. Yang, Q.W. and D.P. performed molecular cloning and the experiments in cell culture. X. Yang, J.M.-L., F.H. and D.P. generated recombinant viruses. X. Yang, F.H., X. Yu, J.M.P. and S.M.C. contributed to the animal studies. F.H. and E.A.H.V. performed the immunofluorescence assays. F.H. conducted the experiments using mouse primary neurons. P.R., Q.W. and D.P. performed the ChIP experiments. A.H.M.N. and G.M.C. developed the methods of deriving mixed neurons from iPSCs. H.S.O. differentiated the iPSCs into sensory neurons with a separate protocol and performed the experiments using the iPSC-derived neurons. J.M.P. provided statistical advice. D.P. and D.M.C. prepared the manuscript. D.P., D.M.K. and D.M.C. provided supervision. All authors approved the manuscript.

Competing interests

A.H.M.N. and G.M.C. are inventors on patent nos. WO2018049382 and WO2018204262 filed by the Presidents and Fellows of Harvard College. Full disclosure for G.M.C. is available on <http://arep.med.harvard.edu/gmc/tech.html>. A.H.M.N. and G.M.C. are co-founders and have equity in GC Therapeutics. Other authors declare no conflict of interest.

Additional information

Extended data is available for this paper at <https://doi.org/10.1038/s41564-020-00860-1>.

Supplementary information The online version contains supplementary material available at <https://doi.org/10.1038/s41564-020-00860-1>.

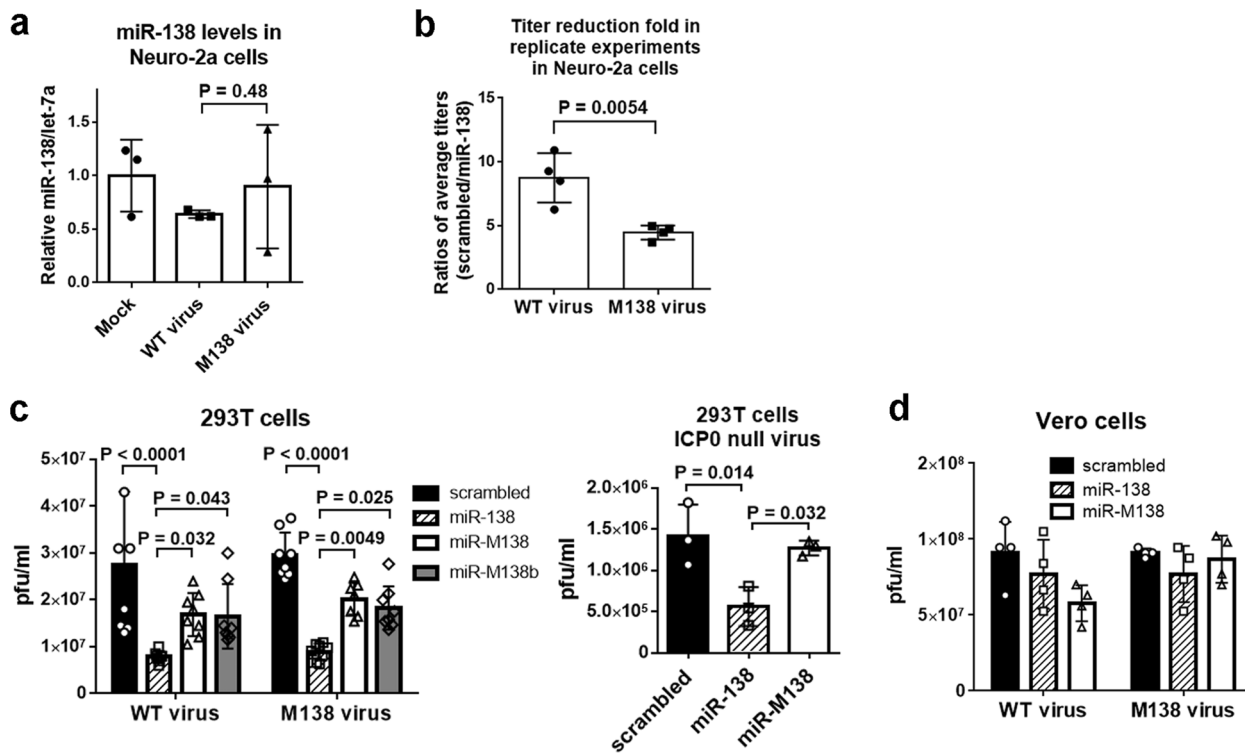
Correspondence and requests for materials should be addressed to D.P.

Peer review information *Nature Microbiology* thanks the anonymous reviewers for their contribution to the peer review of this work.

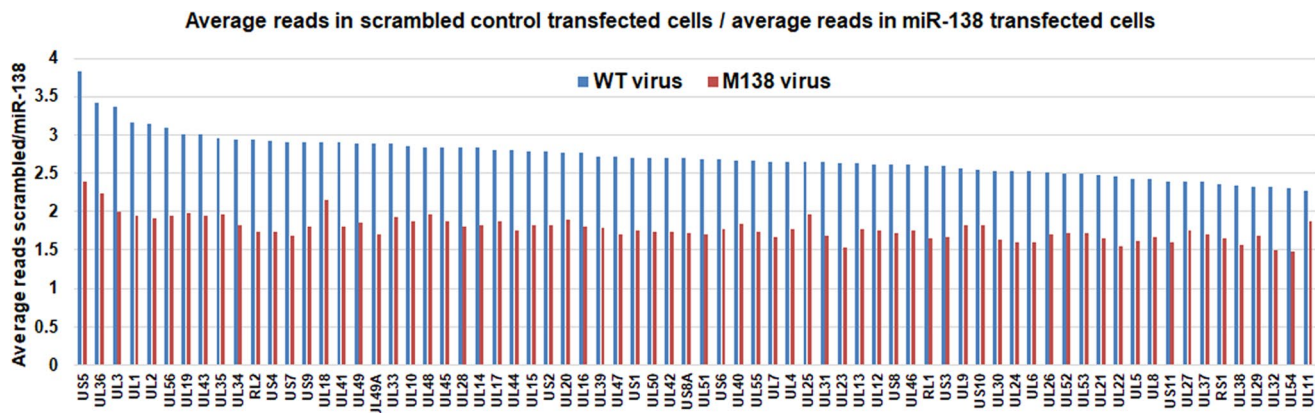
Reprints and permissions information is available at www.nature.com/reprints.

Publisher's note Springer Nature remains neutral with regard to jurisdictional claims in published maps and institutional affiliations.

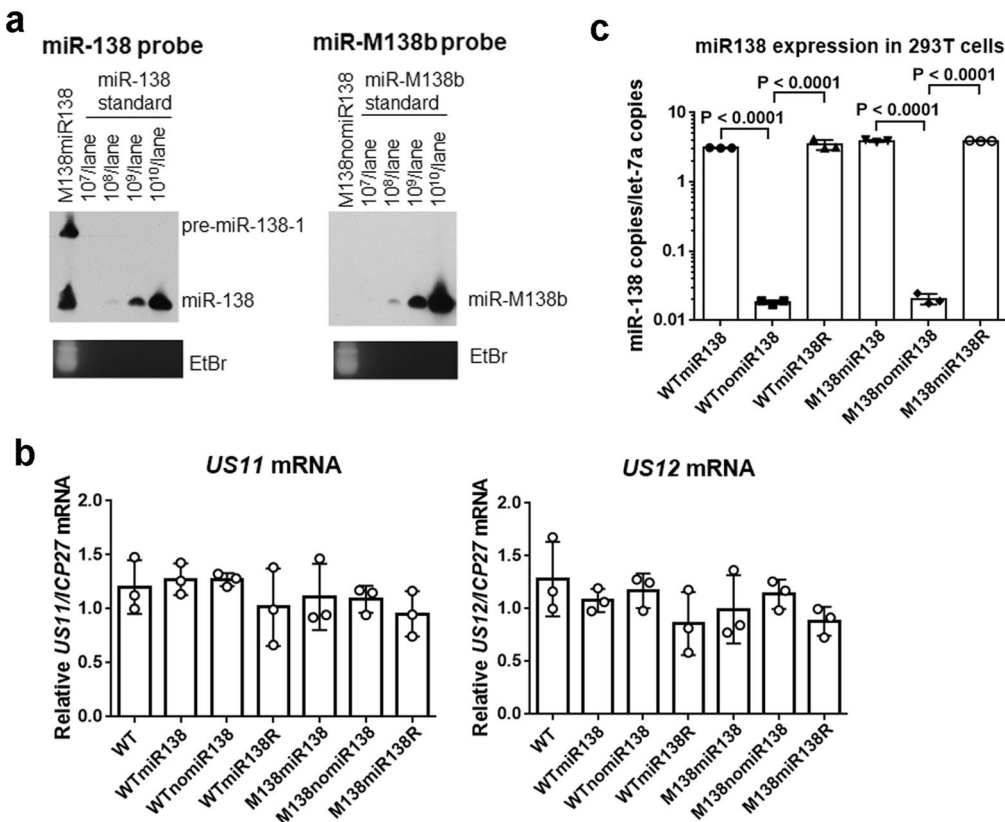
© The Author(s), under exclusive licence to Springer Nature Limited 2021



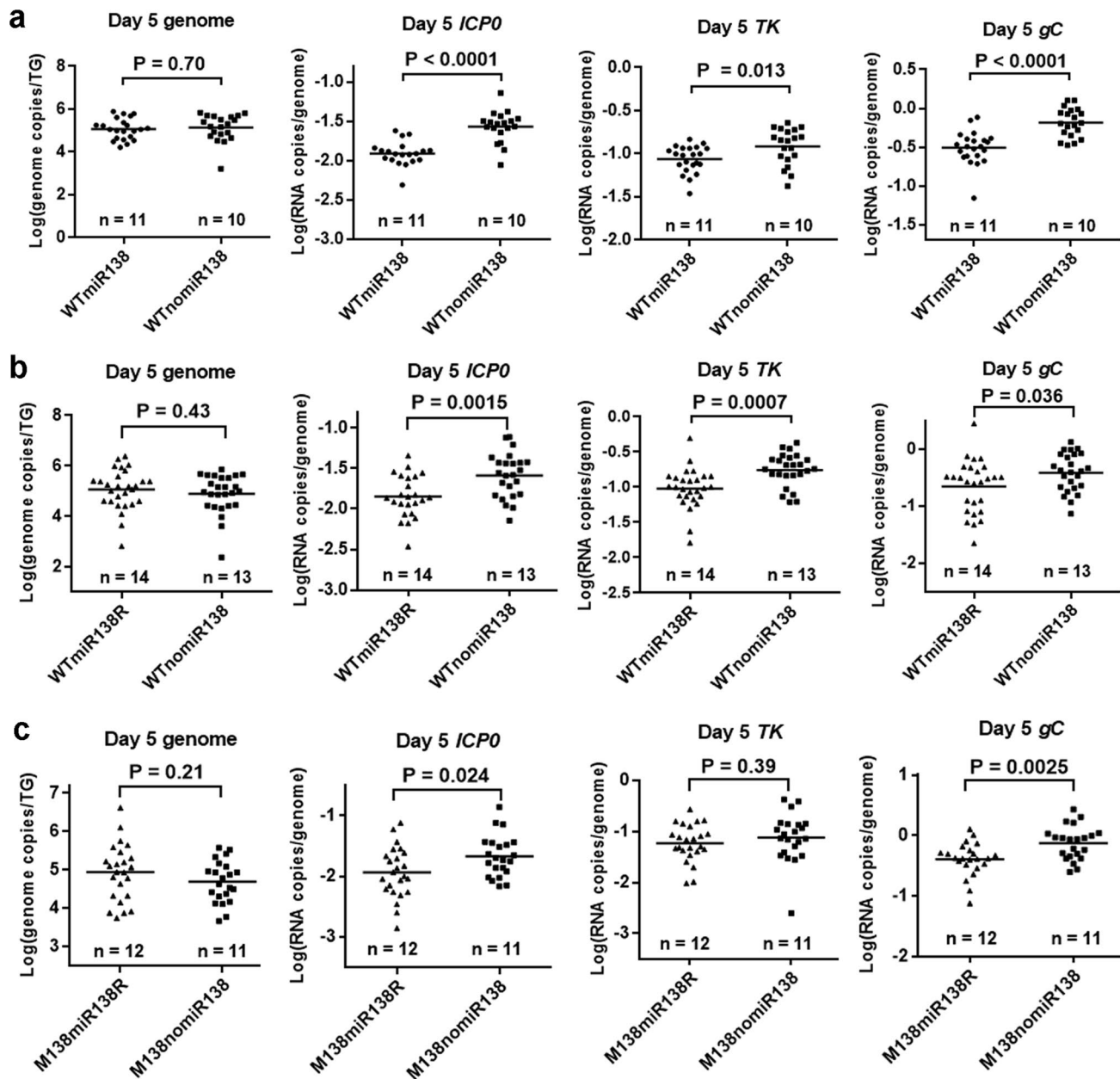
Extended Data Fig. 1 | Additional data about effects of miR-138 on HSV-1 replication. **a**, Neuro-2a cells were mock-infected or infected with the indicated virus ($MOI=5$) for 16 h before qRT-PCR analysis of miR-138 and let-7a levels. **b**, In 4 independent experiments performed as in Fig. 1b, the ratios of the average titers from scrambled transfected cells over those from miR-138 transfected cells were calculated separately for WT and M138 viruses and plotted. **c**, 293T cells were transfected with 40 nM miRNA mimic for 16 h, and then infected with WT or M138 virus (left graph), or 7134 (ICP0-null) virus (right graph) for 48 h ($MOI=0.1$) before viral titer measurements. **d**, Same as **c**, except that Vero cells were infected ($MOI=0.01$) and no significant difference was detected between miR-138 and either of the two controls. For **b**, $n=4$ independent experiments. For other panels, $n=3$ (**a**, **c** right), 4 (**d**) or 8 (**c** left) biologically independent samples per condition. For all panels, data are presented as mean values \pm S.D. and were analyzed by unpaired, two tailed t tests (**a**, **b**), two-way (**c** left, **d**) or one-way (**c** right) ANOVA with Bonferroni's multiple comparisons tests.



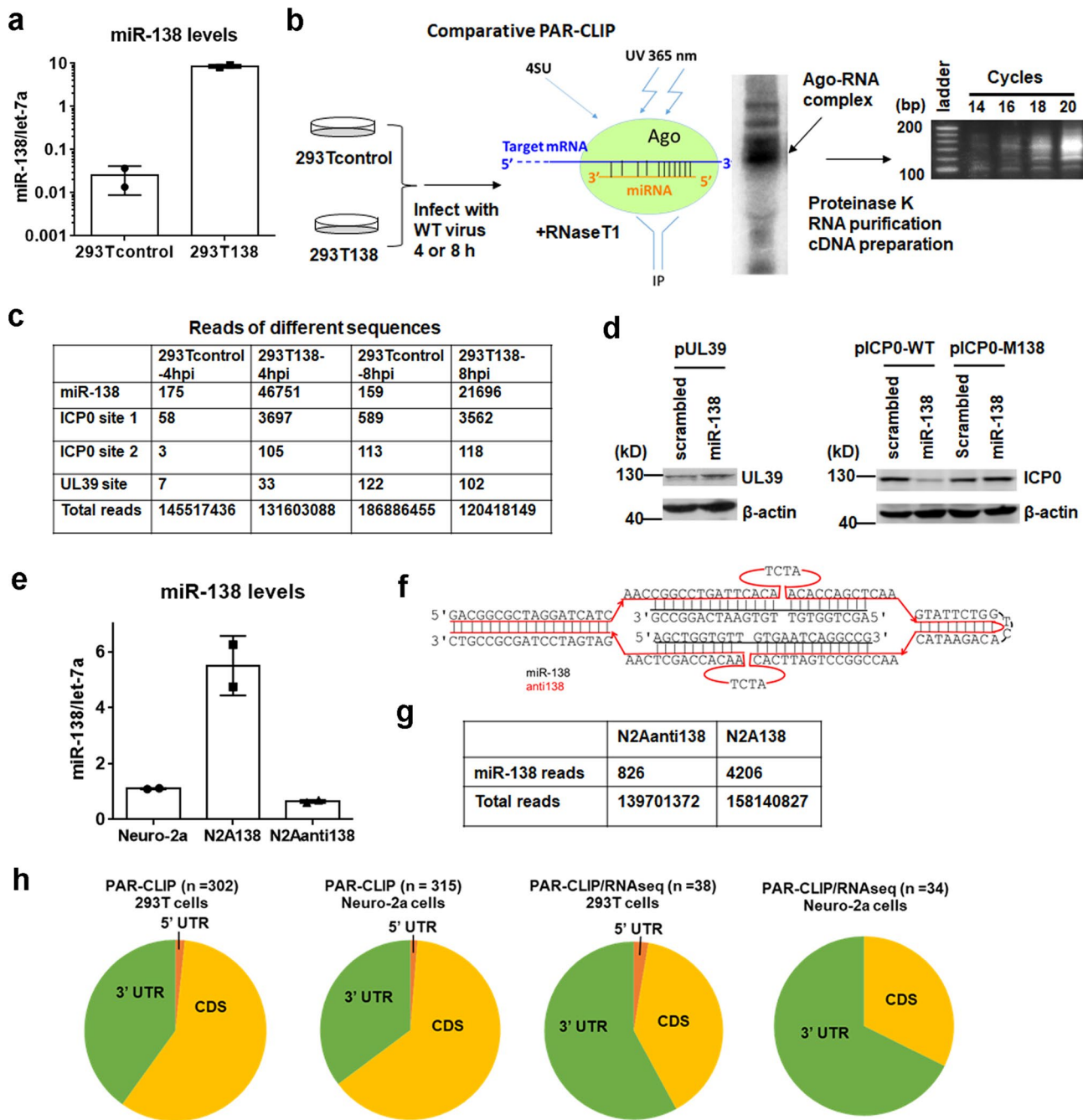
Extended Data Fig. 2 | Global effects of miR-138 on viral gene expression. Same experiment as Fig. 1g, but effects on individual viral transcripts are plotted. Blue and red bars represent data for WT and M138 virus, respectively. n=3 biologically independent samples per condition. Each bar represents the read count mean value for the indicated transcript from scrambled mimic transfected cells (after being normalized to total reads of the sample) divided by that from miR-138 mimic transfected cells.



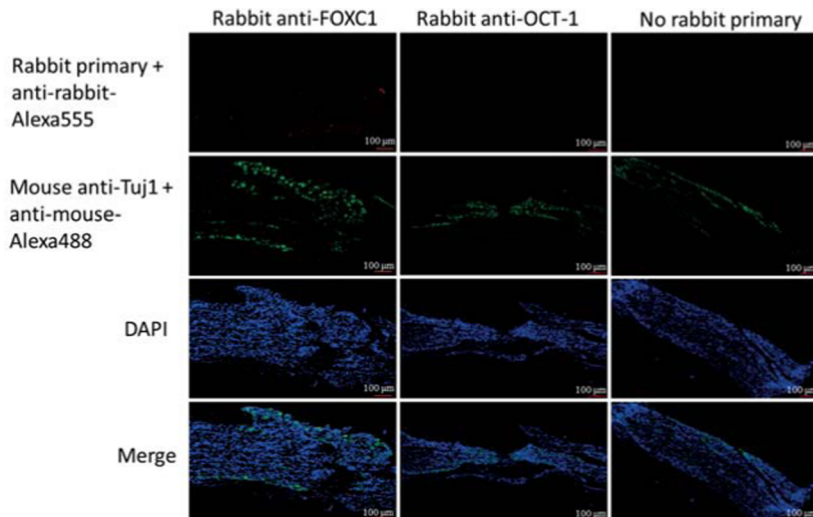
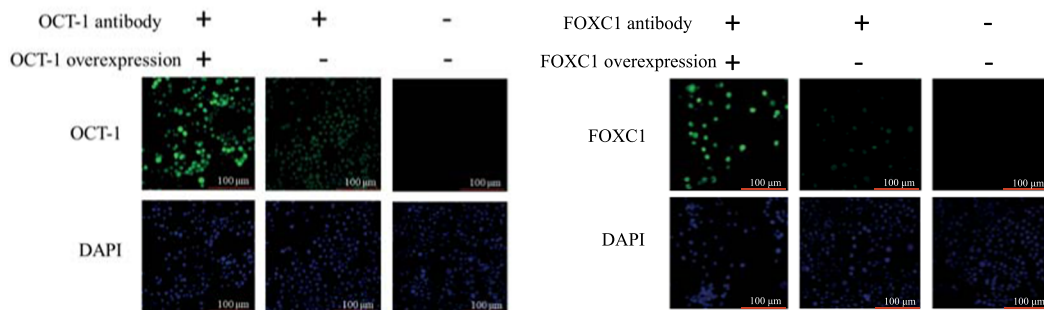
Extended Data Fig. 3 | Expression of miR-138, *US11* and *US12* from recombinant viruses. **a**, 293 T cells were infected with M138miR138 or M138nomiR138 virus (MOI = 5). At 8 hpi, the cells were harvested for RNA purification and Northern blot hybridization. RNA from M138miR138 infected cells was run alongside a dilution series of synthetic miR-138 in the gel and hybridized with a miR-138 probe (left panel). RNA from M138nomiR138 infected cells was run alongside a dilution series of synthetic miR-M138b in the gel and hybridized with a miR-M138b probe (right panel). The integrity of RNA from both samples was verified by ethidium bromide staining, which is shown below the Northern blot images for a set of bands ~80 bases. This experiment was performed once. **b**, Vero cells were infected with the viruses indicated at the bottom at an MOI of 5 and harvested at 8 h post-infection for qRT-PCR analysis of *US11* and *US12* mRNA levels normalized to *ICP27* mRNA levels. **c**, miR-138 expression from 293 T cells infected by the indicated viruses (MOI = 5, 8 h post-infection) as measured by qRT-PCR. For **b** and **c**, n = 3 biologically independent samples and data are presented as mean values ± s.d. Data were analyzed by one-way ANOVA with Bonferroni's multiple comparisons tests.



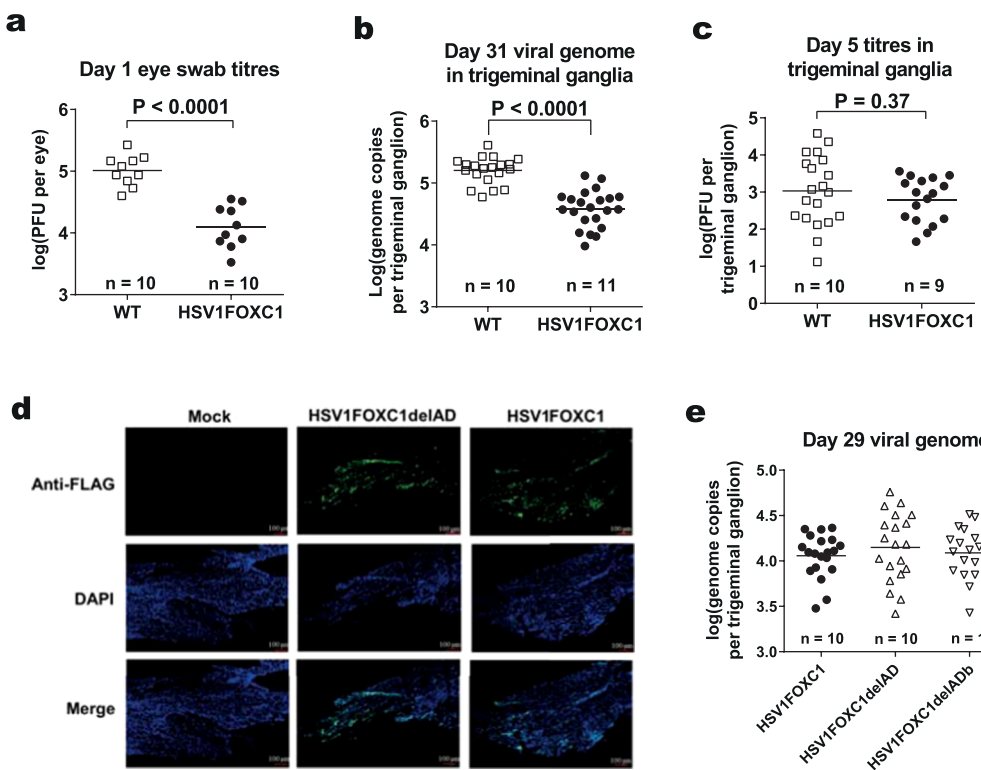
Extended Data Fig. 4 | Additional in vivo data about miR-138 expressing and control recombinant viruses. **a**, Viral DNA and RNA levels in TG infected with WTmiR138 and WTrnomiR138 at 5 dpi. The DNA or RNA molecules measured are labeled at the top of each graph. Viruses are indicated at the bottom. Each point represents a value from one trigeminal ganglion, and the horizontal lines represent the geometric means. The displayed n numbers represent the numbers of mice used per condition. Data were analyzed by two-tailed, unpaired t tests. **b**, Same as **a**, but WTmiR138R and WTrnomiR138 are compared. **c**, Same as **a**, but M138miR138R and M138nomiR138 are compared.



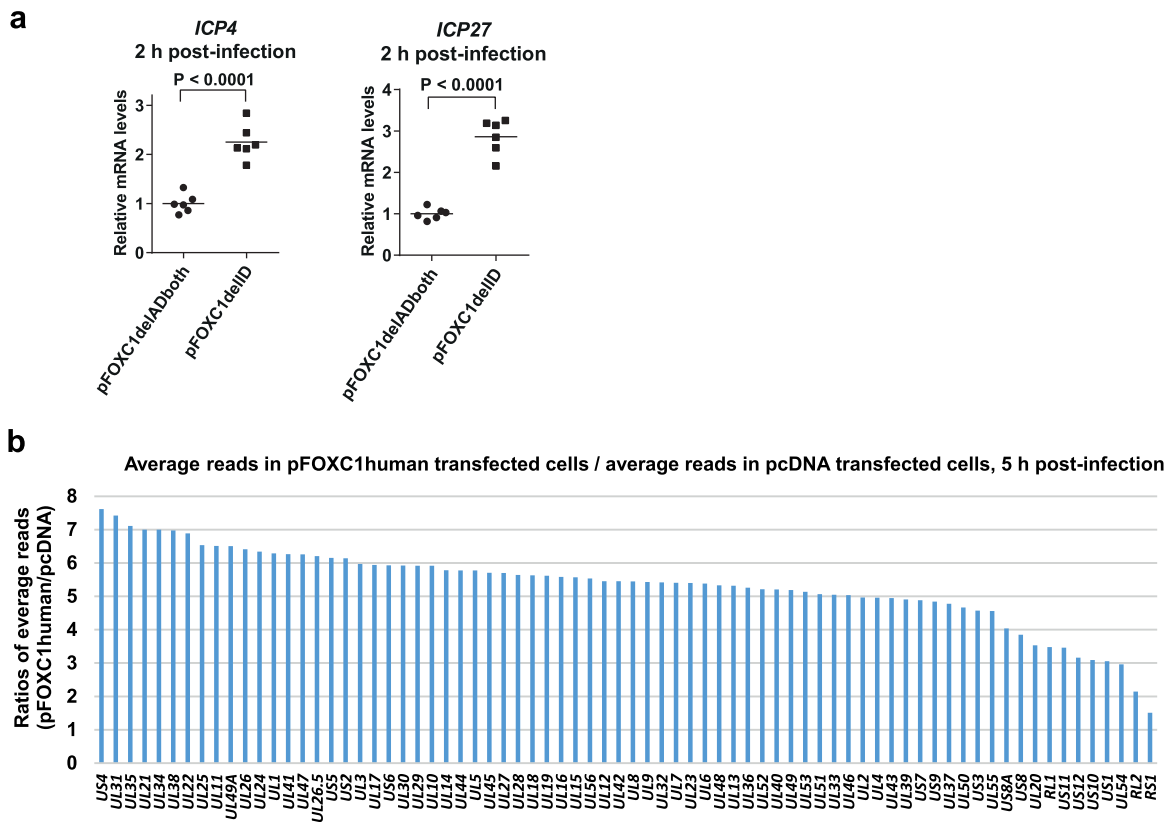
Extended Data Fig. 5 | PAR-CLIP experiments identified viral and host targets of miR-138. **a**, miR-138 expression in 293 Tcontrol and 293T138 cells. **b**, PAR-CLIP procedure for detecting viral targets of miR-138 with, from left to right, a schematic showing the samples, a cartoon showing the crosslinking procedure, a representative autoradiograph of an SDS polyacrylamide gel showing a band corresponding to the Ago-RNA complex, the subsequent steps, and an agarose gel showing PCR amplification of the cDNA library. The experiment was performed once. **c**, Read counts of the indicated sequences from the indicated samples. **d**, 293T cells were co-transfected with 20 nM miRNA mimic and 100 ng/ml plasmid for 48 h before Western blot analysis of FLAG-tagged UL39 using an anti-FLAG antibody and analysis of ICP0 using an ICP0 antibody. This experiment was repeated once with similar results. **e**, miR-138 levels in Neuro-2a, N2A138 and N2Aanti138 cells. **f**, Diagram showing the “anti138” sequence expressed in N2Aanti138 cells. The sequence has a “tough decoy” secondary structure. Red and black horizontal lines represent anti138 and miR-138, respectively. Curved lines above and below the main structure represent bulges (extra nucleotides not bound to miR-138) designed to prevent cleavage. **g**, miR-138 and total read counts in the N2A138 and N2Aanti138 cells in a PAR-CLIP experiment. **h**, Fraction of 5' UTR, CDS or 3' UTR sites in total sites identified by the single PAR-CLIP approach (panels 1 and 2) or the combined PAR-CLIP/RNAseq approach (panels 3 and 4) in 293 T (panels 1 and 3) and Neuro-2a cells (panels 2 and 4). Relative to the single PAR-CLIP approach, the combined approach identified significantly higher fractions of targets with 3' UTR sites ($P=0.034$ and 0.0006 for 293 T and Neuro-2a cells, respectively by Fisher's exact tests). For **a** and **e**, $n=3$ biologically independent samples and data are presented as mean values \pm s.d.

a**b**

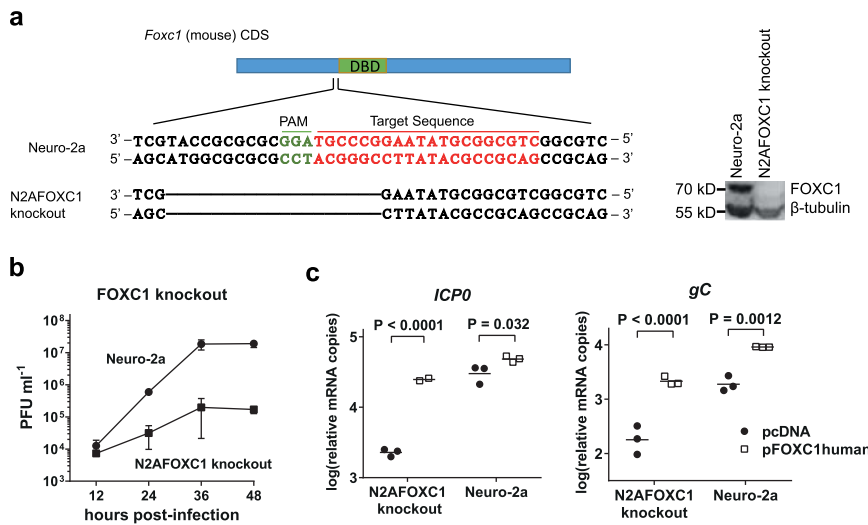
Extended Data Fig. 6 | Low expression of OCT-1 and FOXC1 in mouse TG. **a**, Fixed trigeminal ganglion cryo-sections were stained using an anti-FOXC1 or anti-OCT-1 rabbit primary antibody (red) or without a rabbit primary antibody (control), stained with a mouse anti-Tuj1 antibody (green), and stained with DAPI (blue). Similar results were obtained for OCT-1 using a different OCT-1 antibody (data not shown). This experiment was repeated twice with similar results. **b**, Neuro-2a cells were mock-transfected or transfected with 200 ng/ml OCT-1 or FOXC1 expressing plasmid for 48 h. The cells were then fixed and stained with an anti-OCT-1 or anti-FOXC1 antibody (green) or without a primary antibody, and stained with DAPI (blue). This experiment was repeated once with similar results.



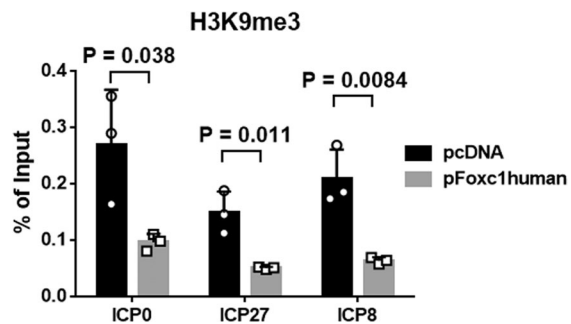
Extended Data Fig. 7 | Additional results with HSV1FOXC1 and HSV1FOXC1delAD viruses. **a**, Mice were infected on the cornea with 2×10^5 PFU per eye of the indicated viruses. Viral titers in eye swabs collected at 1 d post-infection were determined. **b**, Following infection as in a, TG were harvested at 31 d post-infection and analyzed for viral genome levels normalized to mouse *adipsin* gene levels by qPCR. **c**, Following infection as in a, TG were harvested at 5 d post-infection and viral titers in TG were determined. **d**, Following mock infection (left) or infection of mice at the cornea with 2×10^5 PFU per eye of HSV1FOXC1delAD (middle) or HSV1FOXC1 (right), fixed TG cryo-sections were stained by DAPI (blue) and an anti-FLAG antibody (green) that can detect FLAG-tagged FOXC11 and FOXC1delAD proteins. This experiment was performed once. **e**, After corneal inoculation with 2×10^5 pfu/eye of the indicated viruses, mouse TG were harvested at 29 d post-infection and analyzed for viral genome levels normalized to mouse *adipsin* gene levels by qPCR. No significant difference was detected in e. For all panels, the n numbers represent the numbers of mice used per condition. The horizontal lines represent geometrical means. Data were analyzed by two-tailed, unpaired t tests (**a**, **b**, **c**) or one-way ANOVA with Bonferroni's multiple comparisons tests (**e**) with the P values indicated.



Extended Data Fig. 8 | Global effects of FOXC1 on viral gene expression. **a**, Additional data for Fig. 6b. Neuro-2a cells were transfected with 200 ng/ml plasmid for 40 h. KOS was then added (MOI = 2). The cells were incubated at 4 °C for 1 h to allow attachment, washed by PBS and incubated at 37 °C for 2 h before qRT-PCR analysis for the transcript indicated at the top normalized to host GAPDH levels. n = 6 biologically independent samples. The horizontal lines represent mean values. Data were analyzed by two-tailed, unpaired t tests. **b**, Neuro-2a cells were transfected with 200 ng/ml pcDNA or pFOXC1human for 40 h and infected with KOS for 5 h at an MOI of 1 before RNA-seq analysis. n = 3 biologically independent samples. Each bar represents the mean read count for the indicated transcript from pFOXC1human transfected cells (after being normalized by total reads from that sample) divided by that from pcDNA transfected cells.



Extended Data Fig. 9 | FOXC1 is important for HSV-1 replication and gene expression. **a**, Left, *Foxc1* CDS is depicted as a blue box with the DBD in green. Expanded below is the region of deletion in N2AFOXC1 knockout cells, showing sequences in WT and KO cell lines. The PAM sequence required for guide RNA target recognition is shown in green and the target sequence in red. Right, expression of FOXC1 relative to β -tubulin (loading control) in Neuro-2a and N2AFOXC1 knockout cells was analyzed by Western blots. This experiment was repeated twice with similar results. **b**, Neuro-2a and N2AFOXC1 knockout cells were infected with KOS (MOI = 0.5) for the indicated times. Mean viral titers \pm s.d. are shown. **c**, Additional data for Fig. 6e. N2AFOXC1 knockout or Neuro-2a cells were transfected with 400 ng/ml pcDNA or pFOXC1human. 40 h later, the cells were infected with KOS for 5 h at an MOI of 1 before qRT-PCR analyses of the transcript indicated at the top. Horizontal lines represent geometrical means. Data were analyzed by two-way ANOVA with Bonferroni's multiple comparisons tests. For **b** and **c**, $n = 3$ biological independent samples per condition.



Extended Data Fig. 10 | Foxc1 reduced heterochromatin associated with viral genes. Neuro-2a cells were transfected with 500 ng/ml pcDNA or pFoxc1human, as indicated, for 40 h and infected with KOS for 2 h (MOI = 2) before ChIP-qPCR analysis for association of H3K9me3 with the genes indicated at the bottom. n = 3 biologically independent samples. Mean values \pm s.d. are shown. Data were analyzed by two-way ANOVA with Bonferroni's multiple comparisons tests.

Corresponding author(s): Dongli Pan

Last updated by author(s): Nov 11, 2020

Reporting Summary

Nature Research wishes to improve the reproducibility of the work that we publish. This form provides structure for consistency and transparency in reporting. For further information on Nature Research policies, see [Authors & Referees](#) and the [Editorial Policy Checklist](#).

Statistics

For all statistical analyses, confirm that the following items are present in the figure legend, table legend, main text, or Methods section.

n/a Confirmed

- The exact sample size (n) for each experimental group/condition, given as a discrete number and unit of measurement
- A statement on whether measurements were taken from distinct samples or whether the same sample was measured repeatedly
- The statistical test(s) used AND whether they are one- or two-sided
Only common tests should be described solely by name; describe more complex techniques in the Methods section.
- A description of all covariates tested
- A description of any assumptions or corrections, such as tests of normality and adjustment for multiple comparisons
- A full description of the statistical parameters including central tendency (e.g. means) or other basic estimates (e.g. regression coefficient) AND variation (e.g. standard deviation) or associated estimates of uncertainty (e.g. confidence intervals)
- For null hypothesis testing, the test statistic (e.g. F , t , r) with confidence intervals, effect sizes, degrees of freedom and P value noted
Give P values as exact values whenever suitable.
- For Bayesian analysis, information on the choice of priors and Markov chain Monte Carlo settings
- For hierarchical and complex designs, identification of the appropriate level for tests and full reporting of outcomes
- Estimates of effect sizes (e.g. Cohen's d , Pearson's r), indicating how they were calculated

Our web collection on [statistics for biologists](#) contains articles on many of the points above.

Software and code

Policy information about [availability of computer code](#)

Data collection

OPLENIC version X64, 10.1.11276.20180310 (<http://www.oplenic.com>) for image acquisition

Data analysis

Trimmomatic-0.33 (<http://www.usadellab.org/cms/index.php?page=trimmomatic>)
 Tophat2 version 2.1.0 (<https://ccb.jhu.edu/software/tophat/index.shtml>)
 Htseq-count version 0.9.1 (<https://htseq.readthedocs.io/>)
 DESeq2 version 1.30.0 (<https://bioconductor.org/packages/release/bioc/html/DESeq2.html>)
 fastx_clipper version 0.0.13 (http://hannonlab.cshl.edu/fastx_toolkit/)
 bedtools version 2.27.1 (<https://bedtools.readthedocs.io>)
 GraphPad Prism version 7.00 for Windows, GraphPad Software, La Jolla California USA (www.graphpad.com)
 ImageJ version 1.52n (<https://imagej.nih.gov/ij>)

For manuscripts utilizing custom algorithms or software that are central to the research but not yet described in published literature, software must be made available to editors/reviewers. We strongly encourage code deposition in a community repository (e.g. GitHub). See the Nature Research [guidelines for submitting code & software](#) for further information.

Data

Policy information about [availability of data](#)

All manuscripts must include a [data availability statement](#). This statement should provide the following information, where applicable:

- Accession codes, unique identifiers, or web links for publicly available datasets
- A list of figures that have associated raw data
- A description of any restrictions on data availability

HSV-1 strain KOS genome sequence and annotation: GenBank accession number: JQ673480.1

Human (hg19 version) and mouse (mm10 version) genome sequences and annotations were downloaded from the Harvard Medical School Research Computing server (<https://rc.hms.harvard.edu>)

Raw high-throughput sequencing data for RNAseq (Figs. 1f, 3; Extended Data Figs. 2, 8b) and PAR-CLIP (Fig. 3 and Extended Data Fig. 5) experiments have been deposited to the Gene Expression Omnibus (<https://www.ncbi.nlm.nih.gov/geo>) and assigned the identifier GSE127504.

Uncropped full-length Western blot images of all figures in the manuscript and numerical data with statistical analysis are provided as source data.

Field-specific reporting

Please select the one below that is the best fit for your research. If you are not sure, read the appropriate sections before making your selection.

Life sciences Behavioural & social sciences Ecological, evolutionary & environmental sciences

For a reference copy of the document with all sections, see nature.com/documents/nr-reporting-summary-flat.pdf

Life sciences study design

All studies must disclose on these points even when the disclosure is negative.

Sample size	For experiments in cell culture, we have at least 3 biological replicates per condition. For animal experiments, we normally infected 10 to 20 animals per condition to obtain statistical significance. These sample sizes were determined by power analyses using preliminary results showing variation in combination with our past experience of variation (Pan et al, Cell Host Microbe, 15, 446–456, 2014) to ensure detection of significant differences while keeping sample sizes to a minimum.
Data exclusions	Two outlier values were excluded in Fig. 1h. These values are dramatically out of range of normal distributions (>30-fold higher than the averages of the other 4 values). Original data including the outliers are provided as source data. Also, one sample in the HSV1Foxc1 group of Fig. 5i (right panel) did not show any qPCR signal despite strong signals from all other samples, so that sample was excluded. Likewise, a few samples giving no PCR signals in Extended Data Fig. 4 were excluded and are indicated in source data.
Replication	All data presented are reproducible and representative of at least two independent experiments with multiple replicates unless otherwise stated. The high-throughput sequencing experiments were performed once. However, the results regarding the candidate genes identified by the high-throughput sequencing experiments were verified by multiple follow-up experiments as shown in the manuscript.
Randomization	Samples and mice were all randomly allocated into experimental groups.
Blinding	The investigators were not blinded to group allocation during data collection or analysis. Blinding was not required because the data are quantitative and do not require subjective analysis.

Reporting for specific materials, systems and methods

We require information from authors about some types of materials, experimental systems and methods used in many studies. Here, indicate whether each material, system or method listed is relevant to your study. If you are not sure if a list item applies to your research, read the appropriate section before selecting a response.

Materials & experimental systems

- | | |
|-------------------------------------|---|
| n/a | Involved in the study |
| <input type="checkbox"/> | <input checked="" type="checkbox"/> Antibodies |
| <input type="checkbox"/> | <input checked="" type="checkbox"/> Eukaryotic cell lines |
| <input checked="" type="checkbox"/> | <input type="checkbox"/> Palaeontology |
| <input type="checkbox"/> | <input checked="" type="checkbox"/> Animals and other organisms |
| <input checked="" type="checkbox"/> | <input type="checkbox"/> Human research participants |
| <input checked="" type="checkbox"/> | <input type="checkbox"/> Clinical data |

Methods

- | | |
|-------------------------------------|---|
| n/a | Involved in the study |
| <input type="checkbox"/> | <input checked="" type="checkbox"/> ChIP-seq |
| <input checked="" type="checkbox"/> | <input type="checkbox"/> Flow cytometry |
| <input checked="" type="checkbox"/> | <input type="checkbox"/> MRI-based neuroimaging |

Antibodies

Antibodies used

Primary antibodies

ICP0 antibody (Abcam, ab6513), ICP4 antibody (Abcam, ab6514), ICP27 antibody (Virusys, 1113), TK antibody (Santa Cruz, sc-28037), gC antibody (Fitzgerald, 10-H25A), β-actin antibody (Sigma, A5441), Oct-1 antibody (Abcam, ab178869), Foxc1 antibody (Abcam, ab227977), β-tubulin antibody (Tianjin Sungene Biotech, KM9003), mouse anti-Tuj1 antibody (ab78078, Abcam), mouse anti-FLAG antibody (F1804, Sigma), histone H3 (Abcam ab1791), histone H3K9me3 (Abcam ab8898), histone H3K27me3 (Active Motif 39156), normal rabbit IgG (Millipore 12-370), rabbit anti-mouse IgG FC fragment (Jackson Immune Research, 315-005-008), pan Ago antibody (clone 2A8, Millipore, MABE56).

Secondary antibodies

Goat anti-mouse IgG Alexa Fluor 488 (Abcam, ab150117), goat anti-rabbit IgG Alexa Fluor 555 (Cell Signaling Technology, 4413s), goat anti-mouse IgG Alexa Fluor 568 (ThermoFisher, A11004), donkey anti-rabbit IgG Alexa Fluor 405 (Abcam, ab175651), HRP-conjugated goat anti-mouse (SouthernBiotech, 1030-05), HRP-conjugated goat anti-rabbit (SouthernBiotech, 4030-05), and HRP-conjugated rabbit anti-goat antibodies (SouthernBiotech, 6163-05).

Validation

These are all commercially obtained antibodies that had been validated by manufacturers. Validation statements and references

can be found in the manufacturers' websites. In particular, the antibodies for ChIP experiments were frequently used in publications with many references found in their websites. All the antibodies for viral proteins (ICP0, ICP4, ICP27, TK and gC) are frequently used in the HSV-1 field (see, e.g. our previous publication, Pan et al, *Cell Host Microbe*, 15, 446-456, 2014). Moreover, in all infection experiments, mock-infected samples were used as negative controls to exclude reaction to non-virus species and molecular markers were used for protein sizes. In this study we also particularly validated Oct-1 and Foxc1 antibodies. For both Oct-1 and Foxc1, overexpression increased Western blot (Fig. 4b) and immunofluorescence signals (Extended Data Fig. 6b) obtained using these antibodies, and knockout of Foxc1 eliminated Western blot signals obtained using the Foxc1 antibody (Extended Data Fig. 9a).

Eukaryotic cell lines

Policy information about [cell lines](#)

Cell line source(s)

Vero, 293T and Neuro-2a cells were purchased from American Type Culture Collection. 293T138 and 293Tcontrol cell lines were derived from 293T cells in this study as described in Methods. N2A138, N2Aanti138 and N2AFoxc1KO cell lines were derived from Neuro-2a cells in this study as described in Methods. The human iNGN3 induced pluripotent stem cell line was developed in George M. Church (one of our authors) laboratory. A manuscript that fully describes it has been accepted in *Nature Biotechnology* and will be cited when it is published.

Authentication

Vero, 293T and Neuro-2a cells were obtained from ATCC less than four years ago and frozen in aliquots upon arrival. All cells were used under 30 passages from the time of arrival or construction. Because we assumed the cell lines were authenticated by ATCC, further authentication was not conducted. The iNGN3 induced pluripotent stem cells were verified by short tandem repeat profiling (Dana Farber Cancer Institute).

Mycoplasma contamination

All cell lines tested negative for mycoplasma contamination.

Commonly misidentified lines
(See [ICLAC](#) register)

None

Animals and other organisms

Policy information about [studies involving animals; ARRIVE guidelines](#) recommended for reporting animal research

Laboratory animals

Male CD-1 (ICR) mice, six weeks old.

Wild animals

No wild animals were used in this study.

Field-collected samples

No field-collected samples were used in this study.

Ethics oversight

Mouse housing and experimental procedures were approved by Animal Research Committee of Zhejiang University in accordance with national guidelines.

Note that full information on the approval of the study protocol must also be provided in the manuscript.